

Morphologies of caustics studied by catastrophe charged-particle optics

Tom Fraysse,¹ Robin Cours,¹ Hugo Lourenço-Martins,^{1,*} and Florent Houdellier^{1,†}

¹CEMES-CNRS, Université de Toulouse, CNRS, Toulouse, France

(Dated: September 12, 2025)

This paper explores the topologies of caustics observed in instruments that employ charged particles, such as electron and ion microscopes. These geometrical figures are studied here using catastrophe theory. The application of this geometrical theory to our optical situation has enabled us to analytically reproduce the behaviours of various caustics. The interest lies mainly in the universal nature of these results since our treatment requires no prior knowledge of the optical configuration, but only a smart definition of the control space. This universal approach has finally made it possible to extract mathematical relationships between the aberration coefficients of any optical system, which were hidden by the complexity of optical trajectories but revealed by the set of catastrophes in the control space. These results provide a glimpse for future applications of caustics in the development of new corrected optical systems, especially for ions-based devices.

I. Introduction

Everyone has experienced the pleasure of seeing the formation of elaborate geometric shapes from light, whether on a table, a wall, or any other surface after a sunbeam has passed through a transparent material (see Fig. 1(a)). These mesmerizing figures of diverse shapes - commonly referred to as *caustics* - leave no one indifferent [1]. Their profound beauty is further revealed when working with charged-particle devices, such as electron or ion microscopes, where similar complex caustic formations can be observed. Indeed, the observation of the same optical phenomenon with particles of such a different nature - light, electron, or ion (see Fig. 1(a-c)) - points towards the existence of a universal underlying principle.

The Hamiltonian picture of optics and mechanics constitutes an adapted framework for uncovering this principle. Within this framework, the behaviour of any optical or mechanical system can be derived from the mathematical properties of a single function called the *characteristic function* through the principle of least action [2, 3] - the main challenge lying in determining the appropriate characteristic function.

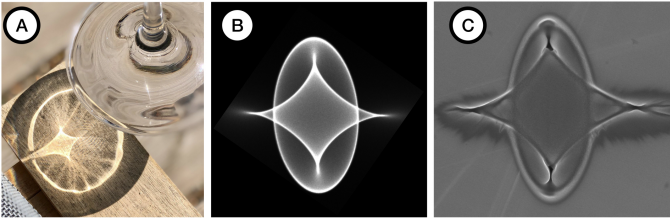


Fig. 1 A caustic observed with (a) a light beam (b) electrons and (c) ions beams

In conventional (light) optics, an appropriate choice for this function corresponds to the optical path length l , as suggested by the Fermat's principle [4]. In that case, the trajectory followed by the light is given by the extremum of l :

$$\frac{\partial l}{\partial x} = \frac{\partial l}{\partial y} = 0 \quad (1)$$

where the variables x, y label the plane transverse to the ray trajectory taken along the optical axis z [5, 6]. The caustics then correspond to the regions of space (x, y) where a high concentration of trajectories that have various initial conditions converge, i.e. have the same function l [7]. Thus, outside the caustic region l is single valued (there is one ray through each point), while inside the caustic l is n -valued (n rays through each point). In other words, the degenerative set of the multi-valued characteristic function will correspond to the location of the caustic surface.

Hamiltonian optics therefore provides a direct operational definition of caustics through the application of the stationarity principle (1), regardless of the physical situation studied [6, 8]. Nonetheless, this approach does not explicit the underlying principle connecting the geometry of caustics to the structure of this multi-valued characteristic functions. In particular, it does not explain why different characteristic functions describing distinct physical systems - may they be mechanical or optical - would lead to the same caustic figures. This is where *catastrophe theory* becomes relevant.

Developed by Rene Thom, this theory deals with the topological structure of smooth functions and their singularities [9–11]. Catastrophe theory has encountered a great success thanks to its efficiency in predicting discontinuous behaviour in systems described by a characteristic function, which span a wide range of practical situations, e.g. the buckling of bridges, liquid-gas phase transition, spin transition in the Ising model or even cellular differentiation [12]. More generally, it applies to almost any situation encountered in modern physics studied under

* hugo.lourenco-martins@cnrs.fr

† florent.houdellier@cnrs.fr

the Hamiltonian pictures, hence to caustics formation [13, 14].

The goal of this paper is to apply catastrophe theory to the study of caustics formation in charged particle optics (CPO) systems. In section II, we start by providing a minimal introduction to catastrophe theory and its application to light optics. In section III, through the application of the principle of least action, we will derive the characteristic function of CPO following the early work of [15]. This will illustrate the great advantage of the Hamiltonian approach, as it enables us to use a common language for charged particles and conventional optics [16]. The physical concepts classically derived from this language (paraxial optics, aberrations theory for instance) will then be identical in all these situations. In section IV, we will apply catastrophe theory to the characteristic function derived in section III. It will lead to the definition of a catastrophe charged-particle optics (CCPO) framework, in which the connection between the structural properties of the characteristic function and the geometry of the caustics become transparent. Eventually, in sections IV C and IV D, we will apply this formalism to derive quantitative relations between the aberration coefficients and the geometrical properties of simple caustics. This final section will highlight the strong potential of CCPO for fast and efficient measurement of the aberration coefficients of CPO systems.

II. A short introduction to catastrophe theory

To be able to mathematically study any physical system using the catastrophe theory, we have to define a so-called generating function $\Phi(X, C)$ [17], which is linked - but not necessarily equal - to the characteristic function. In the following, we will separate the variables of Φ in two sets: the *state variables* x_i and the *control variables* C_i :

$$\begin{cases} X = (x_1, x_2, x_3, \dots, x_s) \\ C = (C_1, C_2, C_3, \dots, C_c) \end{cases} \quad (2)$$

$$(3)$$

where s is called the corank, and c the codimension [13]. In practice, when dealing with physical systems, the state variables are the ones which cannot be controlled by an external stimuli, e.g. the pupil plane coordinates of a ray [18] in optics. Conversely, control variables are the ones which can be adjusted by an external action, e.g. the choice of the image plane in the optical case [19]. The definition of these two sets of variables associated to the correct generating function will be the first task to tackle in order to mathematically define the behaviour of the physical system, and thus properly apply catastrophe theory to the study of its discontinuities. Then, the generating function is usually split in two parts [17] :

$$\Phi(X, C) = g(X) + u(X, C) \quad (4)$$

where g is called the germ and u is the unfolding term, where the control variables appear. The equilibrium surfaces can be determined by taking the derivatives of a generating function describing the dynamical behaviour of the system. Indeed, thanks to the variational principle, the equilibrium surface that results from the differential behaviour's characteristic function being minimized can always be used to describe the dynamical behaviour of any physical phenomenon. Hence, this equilibrium surface will simply correspond to the critical set of Φ , which verifies :

$$\frac{\partial \Phi}{\partial x_1} = \frac{\partial \Phi}{\partial x_2} = \dots = \frac{\partial \Phi}{\partial x_s} = 0 \quad (5)$$

Equation (5) allows us to map the equilibrium surface inside a volume defined by the control and the states variables [20]. For instance if one has two state variables ($X \in \mathbf{R}^2$) and one control variable ($C \in \mathbf{R}$), the equilibrium surface will indeed be a bidimensional surface embedded in a volume $\mathbf{R}^2 \times \mathbf{R}$ [21].

In order to study the caustic as discontinuities in the physical behaviour of our system using the catastrophe theory, we have to compute a subset of the critical set of Φ called the degenerated critical set. To do so, let's consider the Hessian of Φ :

$$H[\Phi] \equiv \left(\frac{\partial^2 \Phi}{\partial x_i \partial x_j} \right)_{i,j} \quad (6)$$

Indeed, mathematically, the degenerated critical set of Φ corresponds to the positions which will satisfy [22]:

$$\det(H[\Phi]) = 0 \quad (7)$$

In that context, caustics are singularities of gradient maps of the form (5) derived from generating functions $\Phi(X, C)$. Catastrophe theory - as developed around Thom's theorem - enables certain caustics, those which are *structurally stable*, to be classified according to their topology [9, 10]. In other words, when the characteristic function of our system is perturbed, the local structure of the caustic remains unaltered because a smooth reversible transformation connects the perturbed and unperturbed caustics known as diffeomorphisms [23]. On the other hand, some non-generic scenario with unique symmetry can lead to a structurally unstable caustics, whose topological type is then altered by perturbations [24].

Thom's theorem states that for every value of the codimension c of the control parameter space $C \in \mathbf{R}^c$, there are only a limited number of structurally stable caustics. In addition, for $c < 5$, it provides seven explicit standard forms for the generating functions called the *elementary catastrophes* [9, 13, 25], classified in Table I.

Catastrophes characterized by $s = 1$ are called cupsoïd, while $s = 2$ leads to so-called umbilic catastrophes.

Name	c	s	$\Phi(X, C)$
Fold	1	1	$\frac{x^3}{3} + Cx$
Cusp	2	1	$\frac{x^4}{4} + C_2 \frac{x^2}{2} + C_1 x$
Swallowtail	3	1	$\frac{x^5}{5} + C_3 \frac{x^3}{3} + C_2 \frac{x^2}{2} + C_1 x$
Elliptic umbilic	3	2	$x_1^3 - 3x_1x_2^2 + C_3(x_1^2 + x_2^2) + C_2x_2 + C_1x_1$
Hyperbolic umbilic	3	2	$x_1^3 + x_2^3 + C_3x_1x_2 + C_2x_2 + C_1x_1$
Butterfly	4	1	$\frac{x^6}{6} + C_4 \frac{x^4}{4} + C_3 \frac{x^3}{3} + C_2 \frac{x^2}{2} + C_1 x$
Parabolic umbilic	4	2	$x_1^4 + x_1x_2^2 + C_4x_2^2 + C_3x_1^2 + C_2x_2 + C_1x_1$

Table I The seven elementary catastrophes classification.

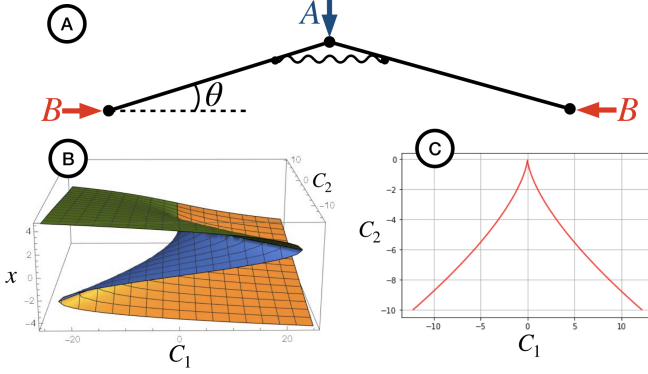


Fig. 2 A: An elastic hinge allowed the two rigid rods that made up the Euler arch to pivot. B force compresses the two ends. Consequently, the angle θ rises. The load called A will be also imposed. The arch gives way upwards (or downwards) at a critical number of these control parameters. B: Plot of the equilibrium positions of the arch using new control and state variables (see text). C: Projection of the equilibrium surface onto the control space depicting the fold catastrophe.

Remarkably, adding more state variables X has no effect on the structurally stable caustics for fixed c . It must be emphasized that - depending on the type of caustic - only one component (x_1) or two (x_1, x_2) of X determine the caustic topology ; all the other components of X can always be transformed to enter $\Phi(X, C)$ quadratically [23], after which they cannot produce singularities when inserted inside equation (5).

A. First example: Euler's arch

We would like to quickly illustrate this method with a situation familiar to any physicist. This mechanical analogy is inspired by Zeeman's groundbreaking work - which has contributed to the understanding of Thom's catastrophe theory - usually called the *Zeeman's machine*, a simple mechanical scenario close to the optical situations studied in this work [26–28].

We begin by describing an Euler arch, as shown on Fig. 2(a), which is made up of two rigid rods pivoting

around a flexible hinge [12, 26]. Let's start by positioning the arch horizontally ($\theta = 0$ on Fig. 2(a)). We then apply a force B at both ends of the arch. For an increasing value of B , the arch will bend upward (or downward). For the sake of the argument, let's assume that the arch buckles upwards, see Fig. 2(a). We then apply a load A on top of the arch. Slowly increasing A , one will eventually reach a critical value for which the arch abruptly snaps into the downward position. To investigate the reason for this behaviour, we need to consider the characteristic function of this problem - which corresponds to the elastic energy V stored in the arch. The latter can be written using a fourth order Taylor expansion as [12]:

$$V = \frac{2\mu + \beta}{12}\theta^4 - \frac{a}{6}\theta^3 - B\theta^2 + A\theta \quad (8)$$

where $\beta = B - 2\mu$ and μ is the elastic constant of the spring. Using the catastrophe theory framework we can define the state variable $x = \theta - \frac{a}{2(2\mu + \beta)}$ and the two new constants C_1 and C_2 - composed using the physical parameters of our system A, B, β, μ - that will be considered as the two control variables of our problem. With those definitions, it is now possible to write the characteristic function according to the cusp generating function - corresponding to one of the seven elementary catastrophe (see Table (I)) :

$$\Phi(x, C_2, C_1) = \frac{x^4}{4} + C_2 \frac{x^2}{2} + C_1 x \quad (9)$$

Then, the arch's equilibrium positions are given by (5):

$$x^3 + C_2 x + C_1 = 0 \quad (10)$$

This cubic equation for x has one or three roots, depending on C_1 and C_2 . This equilibrium condition can be mapped into the space (x, C_1, C_2) and corresponds to a folded surface (Fig. 2(b)), usually called the *catastrophe manifold* [29]. Eventually, the degenerated critical set of Φ can be found by applying equation (7):

$$3x^2 + C_2 = 0 \quad (11)$$

$$\implies x = \pm \sqrt{\frac{-C_2}{3}} \quad (12)$$

To investigate abrupt discontinuities, we can locate the gradient map singularities by using expressions (12). Indeed, they will map in the control parameter space their values causing sudden changes in the system's state parameters. The projection of these positions located on the equilibrium surface onto the control space are called *bifurcation set* [29]. Thom's theorem states that if the generating function is expressed as (9), then the bifurcation set will always be a cusp, as shown in Fig. 2(c), no matter the exact experimental conditions encountered in the laboratory. Hence, by combining equations (10) and (12) we find the parametrization for the cusp :

$$(x, C_2, C_1) = (x, -3x^2, 2x^3) \quad (13)$$

By eliminating the state variable x in (13), one can also compute the equation of the bifurcation set directly in the control space, expressed as a semicubical parabola with a cusp at the origin :

$$4C_2^3 + 27C_1^2 = 0 \quad (14)$$

Fig. 2(c) shows the cusp in control space, for $C_1 \in [-10, 10]$ and $C_2 \in [-10, 0]$.

The previous example aimed at illustrating the overall procedure in the scenario of the most well-known catastrophe defined by a codimension 1 and a corank 2, known as the cusp. Higher codimensions catastrophes will be the focus of our further investigation in the context of charged particle optics. However, their structurally stable caustics will be interpreted using the same mathematical approach.

B. Second example: Catastrophe optics

The specific area of optics where Thom's theory is applied is known as *catastrophe optics*. It was first extensively studied by M. Berry and J. Nye in the context of conventional optics [7, 13]. The purpose of our work is to extend these works to the field of charged particles optics, for applications in electron and ion microscopy. As a preamble, let us briefly review Berry and Nye's equivalent methodology within the framework of standard optics, as given in their corresponding reference works [7, 13, 20, 21].

First of all the pupil plane will be chosen as the state space for our generating function, while the control space will select the position of the observation plane. Following the Fermat's principle and the work of Hamilton, the point characteristic function will be the optical path. It is selected to be the generating function Φ on which the catastrophe theory will be applied. First, this generating function must be expressed in the same structure as one of the seven elementary catastrophes listed in table (I). To do so, we will use the same formalism as the one described by J.F. Nye in [7, 30]. A simple representation of the image side of an optical system is shown on figure

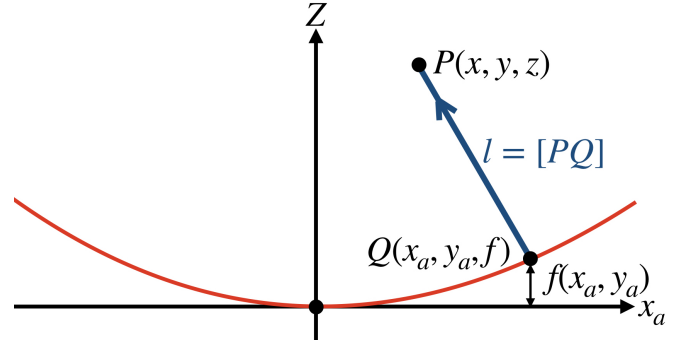


Fig. 3 Optical path l between the exit pupil plane of the system, located in $z = 0$, and the observation plane located at the coordinate Z .

3, where the optical axis is represented by the Z -axis, and its origin is taken at the exit pupil plane.

We are looking for the optical path l between P and Q . Q is a point taken in the wavefront, with coordinate (x_a, y_a, f) , where $f(x_a, y_a)$ is the distance between the pupil plane and the wavefront at the coordinates (x_a, y_a) . In the following, we are going to explore the observation as a function of Z . Points $P(x, y, z)$ which are part of the degenerated critical set of Φ will be called the caustic points. Since we assume that there is no lens between P and Q , the optical path between these two locations corresponds to a straight line expressed as follow :

$$l = \sqrt{(x - x_a)^2 + (y - y_a)^2 + (z - f)^2} \quad (15)$$

We now consider $Z \gg f$ and expand the square root using the far-field approximation, which implies that $Z \gg X - x, Y - y$. Thus, equation (15) can be written at first order as:

$$l \approx z - f + \frac{(x - x_a)^2}{2z} + \frac{(y - y_a)^2}{2z} \quad (16)$$

In this case, the equilibrium conditions (5) can be found using the Fermat's principle (1). After using this principle, the first term in equation (16) will vanish and not contribute to the equilibrium surface. We can then define the generating function Φ - sometimes called Fermat's potential in the literature - as follow [17, 30]:

$$\Phi = z + \frac{x^2 + y^2}{2z} - l \quad (17)$$

$$= f - \frac{x_a^2 + y_a^2}{2z} + \frac{x_a x + y_a y}{z} \quad (18)$$

Then, we admit the following relation that comes from [30]:

$$f(x_a, y_a) = W(x_a, y_a) + \frac{x_a^2 + y_a^2}{2Z_0} \quad (19)$$

where Z_0 is the distance between the paraxial image plane and the pupil plane, and W represents the wavefront

aberrations. Inserting (19) in (18), we obtain the final expression of the generating function :

$$\Phi = W + \left(\frac{1}{2Z_0} - \frac{1}{2z} \right) (x_a^2 + y_a^2) + \frac{x_a x}{z} + \frac{y_a y}{z} \quad (20)$$

Thom's theorem then requires that we express Φ in a canonical form. To do so, one can then define the following three control variables:

$$\begin{cases} C_1 = \frac{x}{z} \\ C_2 = \frac{y}{z} \\ C_3 = \frac{1}{2} \left(\frac{1}{Z_0} - \frac{1}{z} \right) \end{cases} \quad (21)$$

$$\quad (22)$$

$$\quad (23)$$

Besides, as was previously mentioned, the pupil coordinates x_a and y_a correspond to the state variables. The canonical generating function therefore corresponds to:

$$\Phi(x_a, y_a, C_3, C_2, C_1) = W(x_a, y_a) + C_3(x_a^2 + y_a^2) + C_2 y_a + C_1 x_a \quad (24)$$

The critical set of Φ is found by applying (5):

$$\frac{\partial \Phi}{\partial x_a} = \frac{\partial \Phi}{\partial y_a} = 0 \quad (25)$$

The caustics observed in the plane at position z correspond to the regions (x, y) in which a high intensity is created by many rays going through the same point, but coming from different initial pupil positions. According to the catastrophic optics vocabulary, the caustics correspond to the points map in the control space that coincide with the degenerated critical set of the state space [17, 30]. This set verifies equation (7), and therefore the following equation :

$$\frac{\partial^2 \Phi}{\partial x_a^2} \frac{\partial^2 \Phi}{\partial y_a^2} - \left(\frac{\partial^2 \Phi}{\partial x_a \partial y_a} \right)^2 = 0 \quad (26)$$

Using this method, caustic surfaces are obtained in one go, as sets of points that follow (26) and (25), rather than through the computation of each ray's trajectory. This strategy is strictly equivalent to the one described in II A, when replacing the elastic energy by the optical path. In addition, depending on the expression of the wavefront W in (24), the caustic will follow the rules of one of the seven Thom's elementary catastrophes. If a complex wavefront yields a generating function with codimensions and corank outside the validity range of Thom's framework, one needs to follow Arnold's approach, which extends Thom's results to more complex topological generating functions [31].

The primary objective of this introduction was to illustrate the efficiency and generality of the catastrophe theory. Moreover, we have shown why the application of catastrophe theory to conventional optics should be

grounded in Hamilton's theory of characteristic function and Fermat's principle. For charged particle optical systems, the equivalent will be obtained thanks to a modified Lagrangian function and the least action principle.

III. Charged particles optics

A. General approach

As previously introduced, Hamilton demonstrated how the laws of mechanics and optics can be derived by using the mathematical properties of a single characteristic function [2]. In that context, charged-particle optics (CPO) could also be treated using this powerful method of point, mixed and angular characteristic functions [15], which generally depend on six parameters - e.g. the position coordinates of a ray at the object and image areas for the point characteristic functions, or the angular coordinates of a ray at the object and image spaces for the angular characteristic functions. Nevertheless, since an arbitrary trajectory in space is fully characterized by four parameters, Heinrich Bruns demonstrated in 1895 that it is actually preferable to give the characteristic of an optical system as a function of four variables [32]. These modified characteristic functions are generally called *eikonals*. Similar to conventional optics, perturbation methods are usually used to determine the eikonals [33, 34]. These methods, which are based on the perturbation characteristic function approach, provide a useful substitute for the widely used trajectory method, which determine the Lorentz force action on a charged particle by solving the Newton's equation of motion [35].

In the following, we will always assume that the particles travel only in regions which are free of space currents and charges. They will interact with static fields (either electrostatic or magnetostatic) which can be derived from potentials obeying the Poisson equation. Using analytical mechanics we will derive an equivalent of the optical index encountered in conventional optics. Then Hamilton's description of the least action principle will provide us with an equivalent of Fermat's principle, which states that the system minimizes the "optical path" of the charged particles. Later, this definition of the optical path will be used as the generating function to apply Thom's catastrophe theory and Fermat's principle will give us an equilibrium surface [5, 9]. The singularities of this equilibrium surface will then be studied to understand the geometry of the caustics.

B. Hamiltonian picture of charged particles optics

In this section, we will define our generating function by going over the charged particle optics formalism. A dense literature have gone into great detail about this formalism [15, 33, 36] which will be briefly reviewed in the following. In particular, we have chosen to use H. Rose's formalism as our foundation for the next parts, as charged particle optics lacks a standard nomenclature. In this section, a condensed outline of the essential informations needed to fully grasp our application will be presented, while a detailed exposition can be found in [15].

The eikonal approach is based on the analytical mechanics formalism. It is derived using the Hamiltonian H and the Lagrangian \mathcal{L} functions defined using particle kinetic K and potential energies V (of a charged particle inside static fields in our case). In that case the Lagrangian is given simply by the difference between these two energies $\mathcal{L} = K - V$, while the Hamiltonian is the sum of these two energies $H = K + V$ [37]. The action - which is then defined as the integral of the Lagrangian over time - is used to apply the principle of least action [8].

The Lagrangian of a charged particle (an electron in that case) inside an electromagnetic field is explicitly given by [15] :

$$\mathcal{L} = m(v^2 - c^2) - e\mathbf{v} \cdot \mathbf{A} + e\phi \quad (27)$$

where e , m and \mathbf{v} are respectively the charge, the mass [38] and the speed of the electron. ϕ denotes the electrostatic potential and \mathbf{A} is the magnetostatic vector potential, both generated by electromagnetic lenses. Using the Lagrangian, we can define the action W [8] as:

$$W = \int_{t_0}^t \mathcal{L}(\mathbf{r}, \dot{\mathbf{r}}, t) dt \quad (28)$$

where we assumed that the particle goes from \mathbf{r}_0 at t_0 to the point \mathbf{r} at t . Using Legendre transformation, one can write: $L = \mathbf{p} \cdot \dot{\mathbf{r}} - H$, with $\dot{\mathbf{r}} = d\mathbf{r}/dt$. Since, we will discuss only stationary optical system, we obtain:

$$S = W + E(t - t_0) \quad (29)$$

$$= \int_{t_0}^t \mathbf{p} \cdot \dot{\mathbf{r}} dt - \int_{t_0}^t H dt + E(t - t_0) \quad (30)$$

$$= \int_{\mathbf{r}_0}^{\mathbf{r}} \mathbf{p} \cdot d\mathbf{r} \quad (31)$$

with E corresponding to the energy of the system and S the reduced action - or eikonal [15]. Because the optical axis corresponds to the z axis one can define :

$$\tilde{\mathcal{L}} = \mathbf{p} \frac{d\mathbf{r}}{dz} \quad (32)$$

$$\implies S = \int_{z_0}^z \tilde{\mathcal{L}} dz \quad (33)$$

Such as Fermat's principle in conventional optics, the Maupertuis principle in variational mechanics states that [8] :

$$\delta S = 0 \quad (34)$$

Because we are dealing with electromagnetic systems, it will be more convenient to work using complex notations by defining $w = x + iy$, $\bar{w} = x - iy$, $w' = \frac{dw}{dz}$. We moreover set $w_0 = w(z_0)$ since w is a function of z i.e. $w = w(z)$. The equations of motion can be expressed using Euler-Lagrange (EL) formulation of (34) which gives [8] :

$$\left\{ \frac{d}{dz} \left(\frac{\partial \tilde{\mathcal{L}}}{\partial w'} \right) = \frac{\partial \tilde{\mathcal{L}}}{\partial w} \right. \quad (35)$$

$$\left. \frac{d}{dz} \left(\frac{\partial \tilde{\mathcal{L}}}{\partial \bar{w}'} \right) = \frac{\partial \tilde{\mathcal{L}}}{\partial \bar{w}} \right. \quad (36)$$

Expressing (32) using the complex variables one can show:

$$\tilde{\mathcal{L}} = \mathbf{p} \frac{d\mathbf{r}}{dz} \quad (37)$$

$$= p_x x' + p_y y' + p_z \quad (38)$$

$$= \frac{1}{2}(p\bar{w}' + \bar{p}w') + p_z \quad (39)$$

which leads to:

$$\frac{\partial \tilde{\mathcal{L}}}{\partial \bar{w}'} = \frac{1}{2}p \quad (40)$$

where $p = p_x + ip_y$ corresponds to the complex lateral component of the canonical momentum. The variational function δS can be expressed through an integration by part of (32). Then, using EL equations (35) and (36), together with (40), we eventually obtain the following expression [39] :

$$\delta S = \text{Re}(p\delta\bar{w} - p_0\delta\bar{w}_0) \quad (41)$$

leading to the well-known conventional optics equations enabling to express the values of one set of variables (momentum or space variables) with the derivate of the eikonal function relatively to the other set (in object or image space) [4, 6, 40]. S is a function of space coordinates w_0 , \bar{w}_0 , w and \bar{w} in object and image spaces. It then corresponds to the point eikonal which is usually called Hamilton's point characteristic function in conventional optics. Hence, thanks to (41), we can express the momentum coordinates through a simple differentiation of the point eikonal function:

$$\left\{ p_0 = -2 \frac{\partial S}{\partial \bar{w}_0} \right. \quad (42)$$

$$\left. p = 2 \frac{\partial S}{\partial \bar{w}} \right. \quad (43)$$

Other eikonal functions can be expressed from the Legendre transformation of S using (42). For instance the angle-point eikonal function - which depends on the momentum p_0 and \bar{p}_0 in the object space, and the space coordinates w and \bar{w} in the image space - can be expressed as: [6, 15]:

$$\begin{cases} V(p_0, \bar{p}_0, w, \bar{w}) = S + \text{Re}(p_0 w_0) \\ \delta V = \text{Re}(p \delta \bar{w} + \bar{w}_0 \delta p_0) \end{cases} \quad (44)$$

$$(45)$$

In order to express these eikonal functions as a function of electric and magnetic potentials along the charged particles trajectories, we will first define the energy normalized eikonal function $L = S/q_0$, with $q_0 = \sqrt{2em_e\Phi_0^*}$ the normalized momentum linked to the acceleration voltage of the charged particles. Φ_0 is then the potential on the optical axis at z_0 , and $*$ is used to specify when the relativistic correction has to be taken into account. Like for the Lagrangian in (32), we can also define a new variational function μ using the normalized eikonal function as:

$$L = \frac{S}{q_0} = \int_{z_0}^z \mu dz \quad (46)$$

$$\Rightarrow \mu = \frac{1}{q_0} \mathbf{p} \frac{d\mathbf{r}}{dz} \quad (47)$$

By comparison with Fermat's principle, this variational function μ then corresponds to the classical definition of the optical index in conventional optic - but applied to CPO systems [5, 16]. Here, the optical index in CPO doesn't change abruptly at an interface, but can be regarded as the equivalent of a gradient of optical index in conventional optics [15]. Using the expression of the canonical momentum of a charged particle inside an electromagnetic field $\mathbf{p} = m\mathbf{v} - e\mathbf{A}$, one can split the variational function in two optical indices: the electrostatic μ_e and magnetostatic μ_m contributions to the general variational function μ . These two functions can be expressed as follow:

$$\mu_e = \sqrt{\frac{\phi^*}{\Phi_0^*} (w' \bar{w}' + 1)} \quad (48)$$

$$\mu_m = -\frac{e}{q_0} (A_z + \text{Re}(\bar{A}w')) \quad (49)$$

where $A = A_x + iA_y$ corresponds to the complex radial component of \mathbf{A} . We have defined the relativistically-corrected potentials following H. Rose's notations [15]: $m^2 v^2 = 2em\phi^*$, with $v = |\mathbf{v}|$ and $\phi^* = \phi(1 + e\phi/2m_e c^2)$.

C. Polynomial expansion

In order to extract the paraxial and aberrations' contributions to the charged particles trajectories, we have

to perform a polynomial expansion of the two variational functions (48) and (49) with respect to space and momentum variables.

Let's first consider the electrostatic scalar potential ϕ . This potential can be developed using an azimuthal Fourier series in any plane perpendicular to the optical axis (i.e. the z axis) as:

$$\phi = \sum_{\nu=0}^{\infty} \phi_{\nu} \quad (50)$$

where ϕ_{ν} are the harmonic potentials given by the general expression :

$$\phi_{\nu} = \text{Re} \sum_{\lambda=0}^{\infty} a_{\nu\lambda}(z) (w\bar{w})^{\lambda} \bar{w}^{\nu} \quad (51)$$

Since each harmonic potential (51) is a solution of the Laplace equation, one can show that the components $a_{\nu\lambda}(z)$ can be expressed as a function of the potential extracted from the optical axis $\Phi(z) = \phi(x = y = 0, z)$ and its derivatives [15]. One can define the harmonic components $a_{\nu 0}(z) = \Phi_{\nu}(z)$, and insert (51) inside the Laplace equation. After few mathematical manipulations, one can show that any component $a_{\nu\lambda}$ can be expressed as [15]:

$$a_{\nu\lambda} = (-)^{\lambda} \frac{1}{4^{\lambda} \lambda!} \frac{\nu!}{(\lambda + \nu)!} \Phi_{\nu}^{[2\lambda]} \quad (52)$$

where $\Phi_{\nu}^{[i]}$ corresponds to the i^{th} derivative of Φ_{ν} . Then, injecting these expressions into equation (51), we obtain the general expression of the potential expansion:

$$\phi_{\nu} = \sum_{\lambda=0}^{\infty} (-)^{\lambda} \frac{\nu!}{\lambda! (\lambda + \nu)!} \left(\frac{w\bar{w}}{4} \right)^{\lambda} \text{Re}(\Phi_{\nu}^{[2\lambda]}(z) \bar{w}^{\nu}) \quad (53)$$

and:

$$\phi = \sum_{\nu=0}^{\infty} \sum_{\lambda=0}^{\infty} (-)^{\lambda} \frac{\nu!}{\lambda! (\lambda + \nu)!} \left(\frac{w\bar{w}}{4} \right)^{\lambda} \text{Re}(\Phi_{\nu}^{[2\lambda]}(z) \bar{w}^{\nu}) \quad (54)$$

The same operation can be implemented for magnetostatic systems. The static magnetic flux density vector inside a magnetic system is given by $\mathbf{B} = -\nabla\psi = \nabla \wedge \mathbf{A}$. Indeed, the scalar magnetic potential ψ can be used instead of \mathbf{A} for non-saturated magnetic component [41]. Following H. Rose, we define the conjugate part of A noted $\bar{A} = A_x - iA_y$ and the z component of the magnetic vector potential A_z . We express them also using a polynomial expansion of each harmonic components given by the same azimuthal Fourier decomposition procedure as before (see [15] for details). We find:

$$A_z = \sum_{\nu=0}^{\infty} \sum_{\lambda=0}^{\infty} (-)^{\lambda} \frac{\nu!}{\lambda! (\lambda + \nu)!} \left(\frac{w\bar{w}}{4} \right)^{\lambda} \text{Im}(\Psi_{\nu}^{[2\lambda]}(z) \bar{w}^{\nu}) \quad (55)$$

and:

$$\bar{A} = \frac{i}{2} \bar{w} \sum_{\nu=0}^{\infty} \sum_{\lambda=0}^{\infty} (-)^{\lambda} \frac{\nu!}{\lambda!(\lambda + \nu + 1)!} \left(\frac{w\bar{w}}{4} \right)^{\lambda} \Psi_{\nu}^{[2\lambda+1]}(z) \bar{w}^{\nu} \quad (56)$$

here Ψ_{ν} is the analogue of Φ_{ν} - as it corresponds to the value of the scalar magnetic potential along the optic axis $\psi_{\nu}(x=0, y=0, z) = \Psi(z)$, and $\psi = \sum_{\nu=0}^{\infty} \psi_{\nu}$.

In summary, (53), (54), (55) and (56) are simply polynomial expansions where the variables of each polynomial are w , \bar{w} , w' and \bar{w}' . Electron microscopes' optical elements can be regarded as one (or a superposition of different) electrostatic or magnetostatic harmonic components (which could be either complex or real functions) among the five main symmetries given in the following list :

- $\nu = 0$: Round lens (and acceleration voltage)
- $\nu = 1$: Dipolar lens
- $\nu = 2$: Quadrupolar lens (used stigmator)
- $\nu = 3$: Hexapolar lens
- $\nu = 4$: Octopolar lens

When the polynomial expansions (53), (54), (55) and (56) are inserted in (48) and (49), one can write the variational function μ as a polynomial expansion:

$$\mu = \sum_{n=0}^{\infty} \mu^{(n)} \quad (57)$$

where $\mu^{(n)}$ correspond to a polynomial function of degree n - related to the polynomial expansions of the variables w , \bar{w} , w' and \bar{w}' . Within this notation system, the paraxial solutions of a CPO system can be extracted from this expansion using only the components $n \leq 2$.

D. Paraxial solutions of general optical system

We start by considering the three first terms of the polynomial expansion $\mu = \mu^{(0)} + \mu^{(1)} + \mu^{(2)}$. Interested readers may find in the literature an extensive amount of mathematical details related to these developments [15, 33, 42]. Let's start with the expansion of the magnetic component μ_m . We first have to extract from A_z and \bar{A} all the series which will appear in the polynomial expansion of order 2. According to (55) and (56), each polynomial will be defined by terms of power $2\lambda + \nu$ - noted $A_z^{\nu\lambda}$. Hence, within the paraxial solutions, only the terms $A_z^{00}, A_z^{10}, A_z^{20}$ and A_z^{01} have to be considered :

$$\begin{aligned} A_z^{00} &= \text{Im}(\Psi_0(z)) = 0 \\ A_z^{01} &= -\frac{w\bar{w}}{4} \text{Im}(\Psi_0''(z)) = 0 \\ A_z^{10} &= \text{Im}(\Psi_1(z)\bar{w}) \\ A_z^{20} &= \text{Im}(\Psi_2(z)\bar{w}^2) \end{aligned} \quad (58)$$

The same procedure has to be implemented for \bar{A} . Only the term \bar{A}^{00} among all $\bar{A}^{\nu\lambda}$ terms of the polynomial expansion of \bar{A} appear in the paraxial expansion of μ :

$$\begin{aligned} \bar{A}^{00} &= \frac{i}{2} \bar{w} \Psi_0'(z) \\ \Rightarrow \text{Re}(\bar{A}^{00} w') &= \text{Re} \left(\frac{i}{2} \bar{w} \Psi_0'(z) w' \right) \\ \Rightarrow \text{Re}(\bar{A}^{00} w') &= -\text{Im} \left(\frac{1}{2} \Psi_0'(z) \bar{w} w' \right) \end{aligned} \quad (59)$$

One can then insert equation (58) and (59) into relation (49) to find:

$$\mu_m^{(0)} = 0 \quad (60)$$

$$\mu_m^{(1)} = -\frac{e}{q_0} \text{Im}(\Psi_1 \bar{w}) \quad (61)$$

$$\mu_m^{(2)} = \frac{e}{q_0} \text{Im} \left(\frac{1}{2} \Psi_0'(z) \bar{w} w' - \Psi_2(z) \bar{w}^2 \right) \quad (62)$$

The same operation can be performed for the electrostatic part μ_e and leads to [15]:

$$\mu_e^{(0)} = \sqrt{\frac{\Phi_0^*(z)}{\Phi_0^*(z_0)}} \quad (63)$$

$$\mu_e^{(1)} = \frac{\gamma_0}{2\sqrt{\Phi_0^*(z_0)\Phi_0^*(z)}} \text{Re}(\Phi_1(z)\bar{w}) \quad (64)$$

$$\begin{aligned} \mu_e^{(2)} &= \frac{1}{2} \sqrt{\frac{\Phi_0^*(z)}{\Phi_0^*(z_0)}} \text{Re} \left[w' \bar{w}' - \frac{w\bar{w}}{\Phi_0^*(z)} \left(\frac{\gamma_0 \Phi_0''(z)}{4} \right. \right. \\ &\quad \left. \left. + \frac{\Phi_1(z)\bar{\Phi}_1(z)}{8\Phi_0^*(z)} \right) + \frac{\bar{w}^2}{\Phi_0^*(z)} \left(\gamma_0 \Phi_2(z) - \frac{\Phi_1^2(z)}{8\Phi_0^*(z)} \right) \right] \end{aligned} \quad (65)$$

with:

$$\epsilon = \frac{e}{2m_e c^2} \quad (66)$$

$$\gamma_0 = 1 + 2\epsilon \Phi_0(z) \quad (67)$$

$$v_0 = \frac{1}{\gamma_0} \sqrt{\frac{2e\Phi_0^*(z)}{m_e}} \quad (68)$$

$$\Rightarrow \phi^* = \phi + \epsilon \phi^2 \quad (69)$$

where γ_0 is the Lorentz factor and v_0 is the velocity associated to the accelerated potential Φ_0 . Paraxial solutions can be found by inserting the μ polynomial expansion inside the EL equations [8] which leads to:

$$\frac{d}{dz} \frac{\partial \mu}{\partial \bar{w}'} - \frac{\partial \mu}{\partial \bar{w}} = 0 \quad (70)$$

From this operation, we can extract the paraxial differential equation of a general charged particles systems

:

$$\begin{aligned}
& w'' + \frac{\gamma_0}{2\Phi_0^*}(\Phi_0' + iv_0\Psi_0')w' \\
& + \frac{\gamma_0}{4\Phi_0^*} \left(\Phi_0'' + iv_0\Psi_0'' + \frac{\Phi_1\bar{\Phi}_1}{2\gamma_0\Phi_0^*} \right) w \\
& - \frac{\gamma_0}{\Phi_0^*} \left(\Phi_2 + iv_0\Psi_2 - \frac{\Phi_1^2}{8\gamma_0\Phi_0^*} \right) \bar{w} \\
& = \frac{\gamma_0}{2\Phi_0^*}(\Phi_1 + iv_0\Psi_1)
\end{aligned} \tag{71}$$

This equation is a second order partial differential equation with z -dependent coefficients. There is therefore no general analytical solution, and one has to solve it using adapted numerical integrations. We can nevertheless define four independent solutions $w_\mu, \mu = 1, 2, 3, 4$ from the following boundary conditions [15] :

$$\begin{aligned}
w_1(z_0) &= 1, w_1'(z_0) = 0 \\
w_2(z_0) &= i, w_2'(z_0) = 0 \\
w_3(z_0) &= 0, w_3'(z_0) = 1 \\
w_4(z_0) &= 0, w_4'(z_0) = i
\end{aligned} \tag{72}$$

It is then always possible to express any skew rays as a linear combination of these four solutions:

$$w(z) = x_0 w_1(z) + y_0 w_2(z) + x_0' w_3(z) + y_0' w_4(z) \tag{73}$$

In that context, the principal ray corresponds to $w(z_0) = 1$ or i , $w'(z_0) = 0$ boundary conditions while the marginal ray is defined by the second set of boundary conditions $w'(z_0) = 1$ or i , $w(z_0) = 0$.

E. Paraxial solutions of rotational symmetric optical system

Our work focusing mainly on Transmission Electron Microscopes (TEM) and Focused Ion Beam (FIB) instruments, all paraxial solutions will be limited to the action of rotational symmetric lenses. The paraxial contributions of quadrupole lenses through their electrostatic and magnetic second order components $\Phi_2(z)$ or $\Psi_2(z)$ in equation (71) - practically used in TEM and FIB as stigmator components - will be considered as a perturbations of round lenses paraxial solutions. These contributions will correspond to what is known in the literature as axial astigmatism, which shouldn't be confuse with the standard Seidel astigmatism [43]. Then, only Ψ_0 and Φ_0 will be considered in (71). The paraxial equation that will be considered in this work thus becomes:

$$\begin{aligned}
& w'' + \frac{\gamma_0}{2\Phi_0^*}(\Phi_0' + iv_0\Psi_0')w' \\
& + \frac{\gamma_0}{4\Phi_0^*}(\Phi_0'' + iv_0\Psi_0'')w = 0
\end{aligned} \tag{74}$$

Let's re-define the complex variables using an amplitude/phase representation:

$$\chi = -\sqrt{\frac{e}{8m_e}} \int_{z_0}^z \frac{\Psi_0'}{\sqrt{\Phi_0^*}} dz \tag{75}$$

$$w(z) = u(z)e^{i\chi} \tag{76}$$

where χ corresponds to the Larmor rotation of the electrons [15]. We can then work with only one paraxial equation associated to the evolution of the amplitude u :

$$u'' + \frac{\gamma_0\Phi_0'}{2\Phi_0^*}u' + \frac{\gamma_0}{4\Phi_0^*} \left(\Phi_0'' + \frac{e}{2m_e}\Psi_0'^2 \right) u = 0 \tag{77}$$

The principal π and marginal α fundamental solutions of this equation can be calculated using the following boundary conditions:

$$\begin{aligned}
u_\alpha/u_\alpha(z_0) &= 0, u_\alpha'(z_0) = 1 \\
u_\pi/u_\pi(z_0) &= 1, u_\pi'(z_0) = 0
\end{aligned} \tag{78}$$

Eventually, thanks to the initial conditions $w_0 = x_0 + iy_0$ and $w_0' = x_0' + iy_0'$ of any skew ray, the general solution can be written as a simple linear combination:

$$u = w_0' u_\alpha + w_0 u_\pi \tag{79}$$

F. Aberrations

All the terms $n > 2$ encountered in the polynomial expansion of μ correspond to deviations added to the paraxial solution of a rotational symmetric optical system. Nevertheless, in such a rotationally symmetric system, the odd n terms in the μ^n expansion disappear. Thus, the first terms to be considered after the paraxial contributions are the 4th-order terms (i.e. $n = 4$) - known as primary aberrations or Seidel aberrations. In the following, the term *aberrations* will always refer to wavefront aberrations directly given by the eikonals, while, to avoid any confusion, we will always add the term *transverse* to refer to transverse aberrations.

$\mu^{(4)}$ can be written also as a polynomial sum containing five terms known as: spherical, coma, field astigmatism, Petzval curvature and distortion primary aberrations. The expression of each polynomial coefficients can be obtained using the perturbation method originally developed by Seidel for conventional optics and then extended by Glaser and Sturrock, among others, to charged particle optics [34, 43]. The perturbation method required the used of the eikonal polynomial expansions terms $L^{(n)}$ extracted from equation (40) using the $\mu^{(n)}$ terms. The Seidel terms coming from the 4th-order contribution of the eikonal correspond to intrinsic aberrations which appear despite the "real" quality of the lens field. Indeed, they are direct consequences of the non-linear behaviour of geometrical optics laws. However,

in reality, we will have to additionally consider the parasitic aberrations coming from lenses imperfections or misalignments.

Our reference will be always the paraxial solutions considered between the object and Gaussian image planes. The defocus action of a lens can then be defined using a specific second order eikonal term noted $L_d^{(2)}$. The latter corresponds to a difference of second order optical lengths, specifically between the paraxial ray focus at the Gaussian plane and the one considered in a chosen defocused plane. This eikonal linked to the lens defocus is given by [15]:

$$L_d^{(2)} = Re \left(\frac{1}{2} C_{df} |w'_0|^2 \right) \quad (80)$$

where:

$$C_{df} = \int_{z_0}^z \left[\sqrt{\frac{\Phi_0^*}{\Phi_0^*(z_0)}} \left(u_\alpha'^2 + \chi'^2 u_\alpha^2 - \frac{\gamma_0}{4\Phi_0^*} \Phi_0'' u_\alpha^2 \right) + \frac{e\chi'}{q_0} \Psi_0' u_\alpha^2 \right] dz \quad (81)$$

is known as the *defocus*. This expression is correct only for perfect round lenses. However, due to parasitic contributions, some dipolar Ψ_1^p , quadrupolar Ψ_2^p , or even hexapolar fields Ψ_3^p need be considered. Here, the superscript "p" stands for *parasitic*. In practice, to deal with these parasitic contributions, specific electron optics components such as deflectors, first order and second order stigmators, are inserted along the electron paths. Inside a TEM, magnetic optical elements are added to apply dipolar Ψ_1 , quadrupolar Ψ_2 , or hexapolar Ψ_3 fields aiming at compensating their parasitic counterparts respectively $\Psi_1^p, \Psi_2^p, \Psi_3^p$. In FIB instruments, electrostatic elements are employed.

In the following, we will consider L_p to be the eikonal contribution of these parasitic fields and treat it as a perturbation of the rotational symmetric optics eikonal $L^{(2)}$. This means that, in practice, we will always compute the paraxial solutions of (78) instead of using the more general expression given by (72). The multipolar parasitic fields treated as a perturbations of the paraxial solutions will then lead to third order aberrations even in rotational symmetric system - which are added to the fourth ones coming from the standard Seidel intrinsic contributions. Within the framework of transverse aberrations - extracted after differentiating the eikonal function - these contributions will correspond to second order parasitic and third order Seidel aberrations [43].

In the next sections, we will briefly dive into this formalism using the nomenclature extracted from [44].

1. First, second and third order parasitic aberrations

First and second order parasitic aberrations can be expressed using second order variational function given by

equations (60), (61), (62), (63), (64) and (65). Following the nomenclature of [44] and after lengthy mathematical developments - which can be found in detail in [15] - one can define the first and second order eikonal coming from dipole and quadrupole fields as:

$$\begin{aligned} L_p^{(1)} + L_p^{(2)} &= Re \left(A_0 \bar{w}'_0 + \frac{1}{2} A_1 \bar{w}_0'^2 \right) \\ A_0 &= \frac{ie}{q_0} \int_{z_0}^z u_\alpha \Psi_1 e^{-i\chi} dz \\ A_1 &= \frac{2ie}{q_0} \int_{z_0}^z \Psi_2 u_\alpha^2 e^{-2i\chi} dz \end{aligned} \quad (82)$$

The beam deflection A_0 - originating from the dipolar parasitic field Ψ_1 - leads to a tilt of the optical axis. The second parasitic aberration A_1 is called the axial astigmatism (or first order astigmatism) and induces a difference in paraxial focus between the sagittal and meridional directions. Moreover, the orientation of these sagittal and meridional axis will depend on the phase of A_1 , which itself depend on the phase of Ψ_2 and χ . Third order aberrations can be extracted using the same procedure based on the development of the variational function μ and lead to the following expression of the third order eikonal generated by dipolar Ψ_1 and hexapolar Ψ_3 fields:

$$\begin{aligned} L_p^{(3)} &= Re \left(\bar{B}_2 |w'_0|^2 \bar{w}'_0 + \frac{1}{3} A_2 \bar{w}_0'^3 \right) \\ \bar{B}_2 &= -\frac{ie}{4q_0} \int_{z_0}^z dz \left[\frac{1}{2} \Psi_1'' u_\alpha^3 + \Psi_1 \left(u_\alpha^2 u_\alpha' + i\chi' u_\alpha^3 \right) \right] e^{-i\chi} \\ A_2 &= \frac{3ie}{q_2} \int_{z_0}^z \Psi_3 u_\alpha^3 e^{-3i\chi} dz \end{aligned} \quad (83)$$

Here, the B_2 coefficient is known as the axial coma and is influenced by tilt misalignment with respect to the optical axis. This tilt will be induced by the presence of a dipolar field Ψ_1 . The variation in second-order focusing along the three directions that are angularly equally distributed, and located perpendicularly to the optical axis, is physically caused by the A_2 coefficient associated with second-order astigmatism. This second-order astigmatism is generated by the presence of hexapolar component Ψ_3

2. Fourth order Seidel aberrations

Eventually, regarding fourth order contribution to the eikonal, we have to separate the Seidel intrinsic contributions - given by the term $L^{(4)}$ - and the one arising from parasitic contributions included in the term $L_p^{(4)}$. We will restrict our analysis to spherical aberration out of the five Seidel aberrations. This primary aberration is associated to the polynomial term depending to the fourth power of the rays angular coordinate w'_0 . These, fourth order parasitic terms arises from the contribution of quadrupolar fields Ψ_2 . They lead to various kind of effects that

has been extensively studied in the literature [45]. Concerning our study, we will limit the parasitic contribution of quadrupolar field to the star aberration. Then, after heavy mathematical developments detailed in [15], we obtain the following fourth order eikonal expression:

$$L^{(4)} + L_p^{(4)} = \text{Re} \left(\frac{1}{4} C_s |w'_0|^4 + \bar{S}_3 |w'_0|^2 \bar{w}_0'^2 \right) \quad (84)$$

where the spherical aberration coefficient is defined as:

$$C_s = \frac{1}{2} \int_{z_0}^z dz \left[\sqrt{\frac{\Phi_0^*}{\Phi_0^*(z_0)}} \left(- (u_\alpha'^2 + \chi'^2 u_\alpha^2)^2 \right. \right. \\ \left. \left. - \frac{\gamma_0}{2\Phi_0^*} \Phi_0'' u_\alpha^2 (u_\alpha'^2 + \chi'^2 u_\alpha^2) + \frac{1}{16} (\gamma_0 \Phi_0'''' - \frac{\Phi_0''^2}{\Phi_0^*}) u_\alpha^4 \right) \right. \\ \left. - \frac{e}{2q_0} \Psi_0''' \chi' u_\alpha^4 \right] \quad (85)$$

while:

$$\bar{S}_3 = -\frac{ie}{q_0} \int_{z_0}^z dz \left[\frac{\Psi_2''}{6} u_\alpha^4 + \frac{\Psi_2'}{3} (u_\alpha' + i\chi' u_\alpha) u_\alpha^3 \right] e^{-2i\chi} \quad (86)$$

corresponds to the star aberration. Finally, combining all previous eikonal expressions from first to fourth orders, we obtain the total eikonal expansion:

$$L = \text{Re} \left[A_0 \bar{w}_0' + \frac{1}{2} C_{df} |w'_0|^2 + \frac{1}{2} A_1 \bar{w}_0'^2 + \bar{B}_2 |w'_0|^2 \bar{w}_0' \right. \\ \left. + \frac{1}{3} A_2 \bar{w}_0'^3 + \frac{1}{4} C_s |w'_0|^4 + \bar{S}_3 |w'_0|^2 \bar{w}_0'^2 \right] \quad (87)$$

In the following, we will show how this equation can be serve to define the generating function which will then be used to apply the catastrophe theory to CPO.

G. Computational methods

Numerical computations are required to obtain the paraxial solutions and aberration coefficients. We have performed simulations to analyse the data we had obtained specifically using the electron microscope, even though the theory presented above can be used equally to ion and electron optics instruments. Although caustics in ion microscopy is a topic currently being studied, for the sake of this work we will limit our attention to electron microscopy and hence only compute magneto-static potentials inside the optical system as input datas. Hence, following these calculations, the potentials have to be developed and differentiated along the optical axis in order to determine all the multipolar contributions using the expressions (53), (54), (55) and (56). Usually, in that

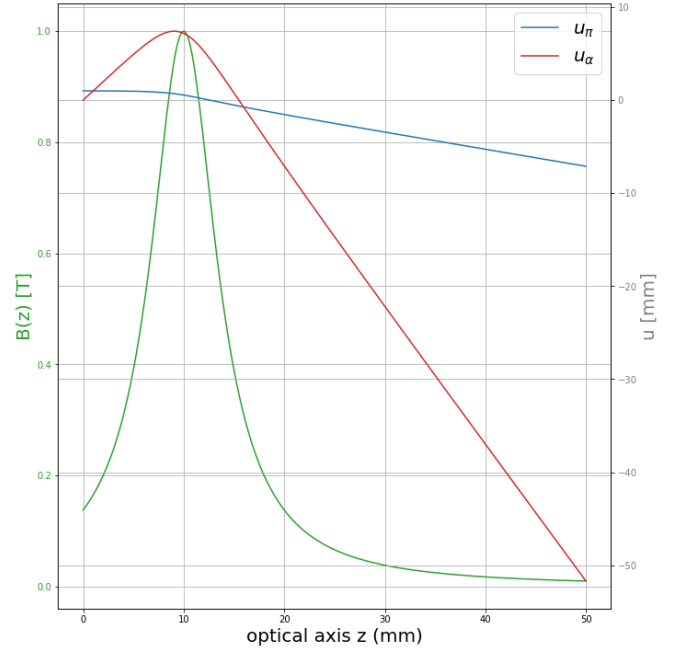


Fig. 4 Paraxial solutions of a magnetic round lens computed using a Runge-Kutta algorithm. A Glaser analytical axial field has been used (in green). u_π, u_α are the two fundamentals paraxial solutions. The optical axis is defined as usual by the condition $u = 0$.

situation we first have to solve the Laplace or Poisson equations inside all optical elements using well established numerical methods such as finite difference (FDM), finite element (FEM), or boundary element (BEM) methods (see [33]). This computational methodology would have to be applied if we wished, for example, to extract quantitative data from an optic with a specific geometrical configuration. However, the aim of this work is primarily conceptual, since we simply wish to provide an explanation of the complex geometrical shapes observed within the TEM's caustics, using catastrophe theory. It is therefore essentially a work on concepts and this is why we have chosen to work with simplified analytical forms of the axial fields. In the case of rotationally symmetric lenses, we have chosen to use the Glaser's representation for the axial magnetic flux density given by [46]:

$$B(z) = \frac{B_0}{1 + \left(\frac{z - z_l}{a} \right)^2} \quad (88)$$

where $B(z) = B_z(x = 0, y = 0, z) = -\Psi_0'$ correspond to the axial magnetic flux density and z_l is the central position of the lens on the optical axis. In that representation B_0 is the maximum strength of the axial magnetic flux density and a is the half peak width of this so-called Glaser's bell-shaped distribution. Furthermore we will consider the multipolar fields Φ_n and Ψ_n components constants along the optical axis. From a physical standpoint, this implies that we will consistently ignore the impact of fringing fields. We should avoid such an approximation if we need to extract quantitative data from an optical

setup that contains a strong multipolar field. However, in our work, we will always consider these fields as only a correction from the rotationally symmetric ones, and conceptually speaking, this approximation will not alter any of the study's qualitative conclusions.

Finally to solve the paraxial equation (74) we used an home-made `Python` code based on Runge-Kutta numerical method (see for instance this introductory book [22]). Figure (4) reports the two paraxial fundamental rays computed by this software using the bell shape Glaser's field as an input field for the equation. This axial field shape has also been represented by the green curve computed using the parameters $z_l = 10\text{mm}$, $a = 4\text{mm}$, $B_0 = 1\text{T}$.

IV. Catastrophe charged-particle optics

The contribution of M. Berry and J. Nye to catastrophe optics - presented in the introduction - will serve as the guideline to extract the generating function of our CPO problem. We start our development with (15) established that in the case of light. As a reminder, we used it to calculate the optical path length between the exit pupil plane, where the wavefront is described, and the caustic observation plane, see Fig. 2(b). In the case of CCPO, instead of using l to build the generating function, we will simply use the normalized point eikonal L as defined by the (46). The optical path found in conventional optics is nevertheless equivalent to this function. The expansion of this function, given by (87) will serve to derive a canonical form of the generating function as prescribed by the catastrophe theory.

A. Charged-particles optical setup

First, it is important to provide an overview of the CPO setup used for our studies. Again, we stress that our analysis will only be performed using the data acquired on the TEM, while the one acquired on the FIB will only be provided as illustration and leave the corresponding details for a future article.

The caustics were acquired on the Hitachi I2TEM microscope of CEMES-Toulouse (In Situ Interferometry Transmission Electron Microscope) [47]. This instrument is based on an HF3300 column of the Japanese manufacturer Hitachi equipped with a 300 keV cold field emission source located before a three condensor lenses system, a double stage objective lens and an imaging aplanatic corrector designed and manufactured by the german company CEOS gmbH [48]. The caustics have been recorded using a CMOS-based detector manufactured by the US company Gatan inc. The schematic overview of the probe forming system, which contains the only components of the larger instrument that will be taken into account for our generating function calculation, is reported in Fig. 5.

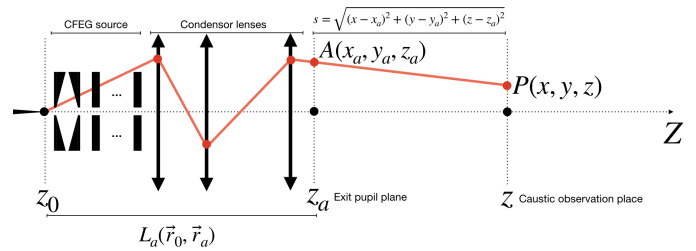


Fig. 5 Electron optical path between the exit pupil plane of the I2TEM illumination system and the caustic observation plane

In the above-described instrument, the optical path will be simply determined by taking into account all the magnetostatic potentials Ψ encountered in the probe forming lens system. In the FIB scenario however, the optical system's electrostatic potential Φ would have to be considered instead. Apart from that, the method described in the next section can be applied exactly as it is.

B. CCPO formalism

1. The generating function

We shall divide the optical path into two separate functions using a geometrical method, which will prove as convenient for defining the generating function. This approach was first presented by H. Rose in [15].

The two geometrical areas are reported on Fig. 5 and will be addressed separately. There, z and z_0 indicate the locations of the caustic observation plane and the electron source, respectively, along the optical axis. The exit pupil plane's coordinate of the probe forming optics is noted z_a . The point $A(x_a, y_a, z_a)$ in the exit pupil plane and the point $Q(x, y, z)$ in the caustic observation plane are connected by a random electron trajectory. In order to simplify our theoretical strategy, we shall consistently consider the exit pupil plane as being outside of any electromagnetic field generated by the optical system.

Combining L_a and s - defined on Fig. 5 - enables us to determine the optical path L as $L = L_a + s$. In this expression, L_a corresponds to the optical path between z_0 and the exit pupil plane z_a , while s corresponds to the one located between the exit pupil plane z_a and z - which is considered in the field-free zone. The calculation of L_a is then done by integrating the variational function μ between z_0 and z_a and by considering the axial magnetic potential and their derivatives along the optical axis (46). The wavefront aberration function is also included in this first function. The second component of the optical path - s - is expressed by taking into account a straight line connecting A and P . In order to eliminate the square root appearing in the expression, we apply the far-field approximation as done for conventional catastrophe optics

in the introduction:

$$s = \sqrt{(x - x_a)^2 + (y - y_a)^2 + (z - z_a)^2} \quad (89)$$

$$\approx z - z_a + \frac{(x - x_a)^2}{2z} + \frac{(y - y_a)^2}{2z} + \frac{z_a^2}{2z} \quad (90)$$

The optical path L_a will be defined by the equation (87). This function is written as a sum of polynomial functions of w'_0 . However, similar to conventional optics, we have to choose the pupil plane coordinates (x_a, y_a) as the states variables for our generating function. In order to express the optical path L_a using the complex pupil plane coordinates $w_a = x_a + iy_a$ we will have first to rewrite it after converting these variables. We have first to set $u_a = u(z_a)$, $u_{\alpha a} = u_{\alpha}(z_a)$ and $\chi_a = \chi(z_a)$. Given that, by definition, the paraxial principal trajectory crosses the optical axis at the centre of the exit pupil plane, with $u_{\pi}(z_a) = 0$, one has:

$$\begin{aligned} u_a &= w'_0 u_{\alpha a} \\ w_a &= u_{\alpha a} e^{i\chi_a} \\ \Rightarrow w'_0 &= \frac{w_a}{u_{\alpha a}} e^{-i\chi_a} \end{aligned} \quad (91)$$

Equation (87) can now be used to express the optical path L_a as the polynomial sum of w_a and its complex conjugate by substituting w'_0 by its expression (91). Specifically, we obtain:

$$\begin{aligned} L_a = \text{Re} & \left[\frac{A_0}{u_{\alpha a}} e^{i\chi_a} \bar{w}_a + \frac{1}{2} \frac{C_{df}}{u_{\alpha a}^2} |w_a|^2 + \frac{1}{2} \frac{A_1}{u_{\alpha a}^2} e^{2i\chi_a} \bar{w}_a^2 \right. \\ & + \frac{\bar{B}_2}{u_{\alpha a}^3} e^{i\chi_a} |w_a|^2 \bar{w}_a + \frac{1}{3} \frac{A_2}{u_{\alpha a}^3} e^{3i\chi_a} \bar{w}_a^3 + \frac{1}{4} \frac{C_s}{u_{\alpha a}^4} |w_a|^4 \\ & \left. + \frac{\bar{S}_3}{u_{\alpha a}^4} e^{2i\chi_a} |w_a|^2 \bar{w}_a^2 \right] \end{aligned} \quad (92)$$

We now expand this expression in order to obtain a x_a, y_a polynomial expression. For clarity, we will proceed with the expansion order per order:

$$L_a = L_a^{(1)} + L_a^{(2)} + L_a^{(3)} + L_a^{(4)} \quad (93)$$

where the first order term can be expanded as:

$$L_a^{(1)} = \text{Re} \left[\frac{A_0}{u_{\alpha a}} e^{i\chi_a} \bar{w}_a \right] \quad (94)$$

$$= \text{Re} \left[\frac{A_0}{u_{\alpha a}} e^{i\chi_a} \right] x_a + \text{Im} \left[\frac{A_0}{u_{\alpha a}} e^{i\chi_a} \right] y_a \quad (95)$$

The second order term is developed as:

$$L_a^{(2)} = \text{Re} \left[\frac{1}{2} \frac{C_{df}}{u_{\alpha a}^2} |w_a|^2 + \frac{1}{2} \frac{A_1}{u_{\alpha a}^2} e^{2i\chi_a} \bar{w}_a^2 \right] \quad (96)$$

$$\begin{aligned} &= \frac{1}{2} \frac{C_{df}}{u_{\alpha a}^2} (x_a^2 + y_a^2) + \text{Re} \left[\frac{1}{2} \frac{A_1}{u_{\alpha a}^2} e^{2i\chi_a} \right] (x_a^2 - y_a^2) \\ &+ \text{Im} \left[\frac{A_1}{u_{\alpha a}^2} e^{2i\chi_a} \right] x_a y_a \end{aligned} \quad (97)$$

The third order term reads:

$$L_a^{(3)} = \text{Re} \left[\frac{\bar{B}_2}{u_{\alpha a}^3} e^{i\chi_a} |w_a|^2 \bar{w}_a + \frac{1}{3} \frac{A_2}{u_{\alpha a}^3} e^{3i\chi_a} \bar{w}_a^3 \right] \quad (98)$$

$$\begin{aligned} &= \text{Re} \left[\frac{\bar{B}_2}{u_{\alpha a}^3} e^{i\chi_a} + \frac{1}{3} \frac{A_2}{u_{\alpha a}^3} e^{3i\chi_a} \right] x_a^3 \\ &+ \text{Im} \left[\frac{A_2}{u_{\alpha a}^3} e^{3i\chi_a} - \frac{\bar{B}_2}{u_{\alpha a}^3} e^{i\chi_a} \right] x_a^2 y_a \\ &+ \text{Re} \left[\frac{\bar{B}_2}{u_{\alpha a}^3} e^{i\chi_a} - \frac{A_2}{u_{\alpha a}^3} e^{3i\chi_a} \right] x_a y_a^2 \\ &- \text{Im} \left[\frac{\bar{B}_2}{u_{\alpha a}^3} e^{i\chi_a} + \frac{1}{3} \frac{A_2}{u_{\alpha a}^3} e^{3i\chi_a} \right] y_a^3 \end{aligned} \quad (99)$$

Finally, the fourth order term can be expanded as:

$$L_a^{(4)} = \text{Re} \left[\frac{1}{4} \frac{C_s}{u_{\alpha a}^4} |w_a|^4 + \frac{\bar{S}_3}{u_{\alpha a}^4} e^{2i\chi_a} |w_a|^2 \bar{w}_a^2 \right] \quad (100)$$

$$\begin{aligned} &= \left(\frac{1}{4} \frac{C_s}{u_{\alpha a}^4} + \text{Re} \left[\frac{\bar{S}_3}{u_{\alpha a}^4} e^{2i\chi_a} \right] \right) x_a^4 \\ &- 2 \text{Im} \left[\frac{\bar{S}_3}{u_{\alpha a}^4} e^{2i\chi_a} \right] x_a^3 y_a \\ &+ \frac{1}{2} \frac{C_s}{u_{\alpha a}^4} x_a^2 y_a^2 - 2 \text{Im} \left[\frac{\bar{S}_3}{u_{\alpha a}^4} e^{2i\chi_a} \right] x_a y_a^3 \\ &+ \left(\frac{1}{4} \frac{C_s}{u_{\alpha a}^4} - \text{Re} \left[\frac{\bar{S}_3}{u_{\alpha a}^4} e^{2i\chi_a} \right] \right) y_a^4 \end{aligned} \quad (101)$$

Following the formalism of J. Nye [7, 21], the Fermat's potential Φ_f - which will be the ground on which the generating function will be built - can now be expressed using the formula :

$$\Phi_f = L_a + \frac{x_a^2 + y_a^2}{2z} - \frac{xx_a + yy_a}{z} \quad (102)$$

Finally, in order to write down the generating function, it's necessary to display all the polynomials define by the different powers of the variables (x_a, y_a) . Gathering all the orders previously developed in one expression, we find the Fermat's potential Φ_f :

$$\begin{aligned}
\Phi_f = & \left(\operatorname{Re} \left[\frac{A_0}{u_{\alpha\alpha}} e^{i\chi_a} \right] - \frac{x}{z} \right) x_a + \left(\operatorname{Im} \left[\frac{A_0}{u_{\alpha\alpha}} e^{i\chi_a} \right] - \frac{y}{z} \right) y_a + \left(\frac{1}{2} \frac{C_{df}}{u_{\alpha\alpha}^2} + \frac{1}{2z} \right) (x_a^2 + y_a^2) \\
& + \operatorname{Re} \left[\frac{1}{2} \frac{A_1}{u_{\alpha\alpha}^2} e^{2i\chi_a} \right] (x_a^2 - y_a^2) + \operatorname{Im} \left[\frac{A_1}{u_{\alpha\alpha}^2} e^{2i\chi_a} \right] x_a y_a + \operatorname{Re} \left[\frac{\bar{B}_2}{u_{\alpha\alpha}^3} e^{i\chi_a} + \frac{1}{3} \frac{A_2}{u_{\alpha\alpha}^3} e^{3i\chi_a} \right] x_a^3 \\
& + \operatorname{Im} \left[\frac{A_2}{u_{\alpha\alpha}^3} e^{3i\chi_a} - \frac{\bar{B}_2}{u_{\alpha\alpha}^3} e^{i\chi_a} \right] x_a^2 y_a + \operatorname{Re} \left[\frac{\bar{B}_2}{u_{\alpha\alpha}^3} e^{i\chi_a} - \frac{A_2}{u_{\alpha\alpha}^3} e^{3i\chi_a} \right] x_a y_a^2 - \operatorname{Im} \left[\frac{\bar{B}_2}{u_{\alpha\alpha}^3} e^{i\chi_a} + \frac{1}{3} \frac{A_2}{u_{\alpha\alpha}^3} e^{3i\chi_a} \right] y_a^3 \\
& + \left(\frac{1}{4} \frac{C_s}{u_{\alpha\alpha}^4} + \operatorname{Re} \left[\frac{\bar{S}_3}{u_{\alpha\alpha}^4} e^{2i\chi_a} \right] \right) x_a^4 - 2 \operatorname{Im} \left[\frac{\bar{S}_3}{u_{\alpha\alpha}^4} e^{2i\chi_a} \right] x_a^3 y_a + \frac{1}{2} \frac{C_s}{u_{\alpha\alpha}^4} x_a^2 y_a^2 - 2 \operatorname{Im} \left[\frac{\bar{S}_3}{u_{\alpha\alpha}^4} e^{2i\chi_a} \right] x_a y_a^3 \\
& + \left(\frac{1}{4} \frac{C_s}{u_{\alpha\alpha}^4} - \operatorname{Re} \left[\frac{\bar{S}_3}{u_{\alpha\alpha}^4} e^{2i\chi_a} \right] \right) y_a^4
\end{aligned} \tag{103}$$

By comparing this expression to the canonical form of the seven catastrophes, one can understand that all aberration coefficients will have to be treated as control variables. However, in this first work, we have chosen to restrict our analysis to the codimension that has already been covered by R. Thom's and V. Arnold's works and, as a consequence we have decided to discard the star aberration S_3 from (103). Indeed, if one includes this aberration the generating function becomes excessively complex. Nevertheless, given that our CPO system is mainly limited by the spherical aberration of the condensor lenses, this approximation remains reasonable. To fit our expression within the canonical catastrophes (see table I) - which does not exhibits coefficients in the germ polynomial expressions - the Fermat's potential (103) has to be divided by the highest order coefficient of the expansion, which corresponds to the spherical aberration. Eventually, we obtain the final expression for the generating function Φ :

$$\begin{aligned}
\Phi(x_a, y_a, C_1, C_2, C_3, C_4, C_5, C_6, C_7, C_8, C_9) = \\
C_1 x_a + C_2 y_a + C_3 (x_a^2 + y_a^2) + C_4 (x_a^2 - y_a^2) + C_5 x_a y_a \\
+ C_6 x_a^3 + C_7 x_a^2 y_a + C_8 x_a y_a^2 + C_9 y_a^3 + x_a^4 + 2x_a^2 y_a^2 + y_a^4
\end{aligned} \tag{104}$$

in which the following control variables have been defined:

$$C_1 = 4 \left(\operatorname{Re} \left[u_{\alpha\alpha}^3 \frac{A_0}{C_s} e^{i\chi_a} \right] - \frac{x}{z C_s} u_{\alpha\alpha}^4 \right) \tag{105}$$

$$C_2 = 4 \left(\operatorname{Im} \left[u_{\alpha\alpha}^3 \frac{A_0}{C_s} e^{i\chi_a} \right] - \frac{y}{z C_s} u_{\alpha\alpha}^4 \right) \tag{106}$$

$$C_3 = 2 \left(u_{\alpha\alpha}^2 \frac{C_{df}}{C_s} + \frac{u_{\alpha\alpha}^4}{z C_s} \right) \tag{107}$$

$$C_4 = 2 \operatorname{Re} \left[u_{\alpha\alpha}^2 \frac{A_1}{C_s} e^{2i\chi_a} \right] \tag{108}$$

$$C_5 = 4 \operatorname{Im} \left[u_{\alpha\alpha}^2 \frac{A_1}{C_s} e^{2i\chi_a} \right] \tag{109}$$

$$C_6 = 4 \operatorname{Re} \left[u_{\alpha\alpha} \frac{\bar{B}_2}{C_s} e^{i\chi_a} + \frac{u_{\alpha\alpha}}{3} \frac{A_2}{C_s} e^{3i\chi_a} \right] \tag{110}$$

$$C_7 = 4 \operatorname{Im} \left[u_{\alpha\alpha} \frac{A_2}{C_s} e^{3i\chi_a} - u_{\alpha\alpha} \frac{\bar{B}_2}{C_s} e^{i\chi_a} \right] \tag{111}$$

$$C_8 = 4 \operatorname{Re} \left[u_{\alpha\alpha} \frac{\bar{B}_2}{C_s} e^{i\chi_a} - u_{\alpha\alpha} \frac{A_2}{C_s} e^{3i\chi_a} \right] \tag{112}$$

$$C_9 = -4 \operatorname{Im} \left[u_{\alpha\alpha} \frac{\bar{B}_2}{C_s} e^{i\chi_a} + \frac{u_{\alpha\alpha}}{3} \frac{A_2}{C_s} e^{3i\chi_a} \right] \tag{113}$$

Consequently, even when considering the simplest scenario conventionally encountered during TEM experiments, the codimension of our generating function is 9 - a scenario beyond the seven elementary catastrophes studied by Thom's catastrophe theory. We have therefore to consider the extension of the catastrophe theory developed by V. Arnold [10]. Specifically, the germ of our generating function is:

$$g(x_a, y_a) = x_a^4 + 2x_a^2 y_a^2 + y_a^4 \tag{114}$$

Thus, our generating function corresponds to the so-called X^9 catastrophe of Arnold's theory, which is characterized by the germ $g = x_a^4 + K x_a^2 y_a^2 + y_a^4$ with $K = 2$ [49, 50].

The X^9 catastrophe can have various shapes and geometry depending on the values of the control variables. Nevertheless, based on our observations, the X^9 catastrophe seem to fit all measured TEM caustics topologies, therefore we have chosen to base all of our investigation on this generating function. To visually illustrate our strategy, we report on Fig. 6 a qualitative comparison between one caustic observed in the I2TEM using a strong A_2 aberration - applied using short hexapoles located between the condensor lenses - and one of the possible X^9 symmetry simulated using our code based on this work and strongly inspired from a situation described in J. Nye's book [7].

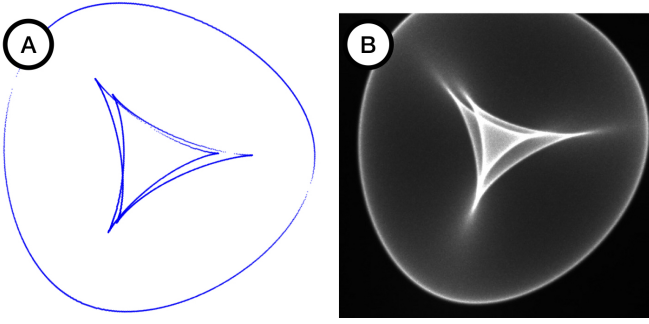


Fig. 6 Left : Simulated caustics projected using a X^9 generating function (inspired by Nye's pioneering work [7]). Right : Caustics taken using the I2TEM instrument.

2. Caustics

The stationary conditions are obtained by applying (25) to Φ :

$$\frac{\partial \Phi}{\partial x_a} = \frac{\partial \Phi}{\partial y_a} = 0 \quad (115)$$

This operation is used to define our system's equilibrium surface, from which any possible trajectories of a charged particle can be derived. In particular, as shown in section II, the caustics are then given by the singularities of this surface. The latter can be found by calculating the roots of the Hessian determinant:

$$\frac{\partial^2 \Phi}{\partial x_a^2} \frac{\partial^2 \Phi}{\partial y_a^2} - \left(\frac{\partial^2 \Phi}{\partial x_a \partial y_a} \right)^2 = 0 \quad (116)$$

We shall therefore obtain the observed caustics from the projection of all singularities encountered in the equilibrium surface onto the control space.

However, equation (116) presents an issue since the Hessian's determinant is a fourth-order polynomial function. As a result, in most situations, it will be impossible to obtain analytical solutions for the Hessian determinant's roots.

Numerical computations constitute one possible solution that we will use to solve this issue. The aberration coefficients could indeed be computed from Glaser's analytic model of the axial magnetic field of round lenses, as presented in section (III). Additional quadrupoles Ψ_2 or hexapoles Ψ_3 field strengths can also be defined analytically by neglecting all the fringing field effects [51]. The knowledge of these aberrations enable the computation of the control variables using equation (105) to (113). The Hessian determinant equation $\det(H) = 0$ (116) is then solved using an home-made Python code employing several numerical approximations.

Nevertheless, we will show in the next section that - in some specific situations - one can derive exact analytical solutions of $\det(H) = 0$. These expressions will enable us to establish relationships between the aberrations and

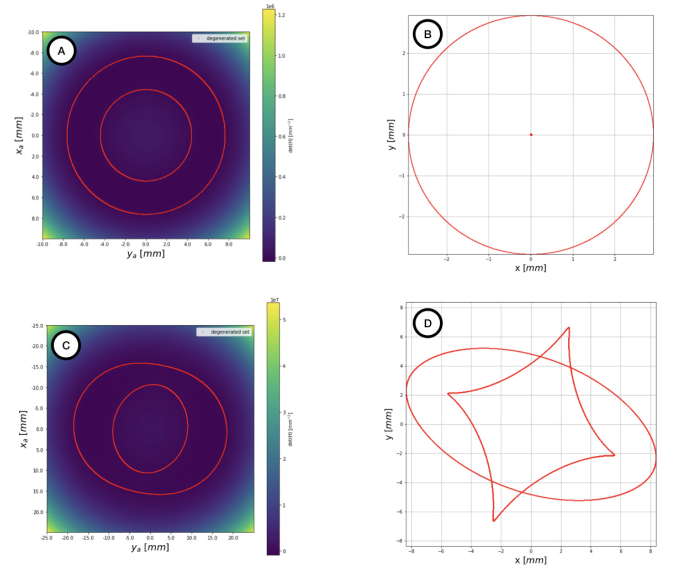


Fig. 7 A : Hessian determinant and B : caustic observed in the observation plane z . calculation are realised for a pure rotationally symmetric configuration. C: hessian determinant and D : caustic determined after a quadrupole Ψ_2 field component was added.

the caustic shape. The latter will reveals complex relations hidden inside the formalism of charged particles optics which would have been impossible to easily extract without the catastrophe theory formalism.

C. Application: Numerical derivation of caustic geometry from optical calculations

We begin by solving equation (116) using a generating function whose coefficients were derived numerically from integral expressions of the aberrations. Estimations have been performed for the optical system depicted on Fig. 5 corresponding to the illumination system of the I2TEM microscope. In addition, the axial field of the condenser lenses are expressed using Glaser's method. With these conditions, derivations can therefore be analytically performed very easily. Thus, procedures described in section III G are applied to determine the paraxial solutions and the aberrations coefficients. We will describe the results of these calculations in the rest of this section.

Fig. 6(a) shows the Hessian determinant mapped as a function of the pupil plane coordinates when considering only rotationally symmetric components of the fields i.e. $\Psi_0 \neq 0$ and $\Psi_1 = \Psi_2 = \dots = 0$. The spherical aberration coefficient C_s is determined with (85), and we consider no defocus $C_{df} = 0$. In that case the generating function contains only the first three control variables C_1, C_2, C_3 . The Hessian determinant can moreover be calculated with setting $C_1, C_2 = 0$ in Φ since these two control variables will nevertheless disappear due to the double derivative in

(116). In practice, the zeros of the Hessian determinant - i.e. the degenerated set - are numerically extracted from the sign changes in the function when mapping it on the pupil plane space (x_a, y_a) . These points are marked by the red dots on the $\det(H) = 0$ map (see Fig. 7(a)).

One can observe two subsets of these roots mapped along two circles of different radius centred on $(0, 0)$. Applying Fermat's principle (115) for the rays defined by the two degenerative sets in the pupil plane, we can now map the caustic in the control space C_1, C_2 , which is equivalent to the (x, y) usual space. To plot the caustic on Fig. 6(b) we have set $z = z_g$ for the Gaussian plane (i.e. $C_{df} = 0$). A typical beam shape - that has a first caustic point at $(0, 0)$ and a second caustic that corresponds to a circle of $(0, 0)$ centre - is observed. The scale is given in mm since we neglected the effect of the demagnification coming from the objective lens located after the condenser lenses.

In a second step, we add a small quadrupolar field $\Psi_2 = 0.01$ T/m corresponding to an order of magnitude usually encountered in condenser stigmators. The two-fold astigmatism A_1 can then be estimated using the expression (82) by integrating the paraxial trajectory computed over our rotationally symmetric system. The Hessian determinant is then mapped onto the pupil plane space and the degenerated sets are numerically estimated as previously done. Fig. 6(c) again displays two subsets with a slight elliptical distortion. Going back to the control space (x, y) using the Fermat's principle and setting $z = z_g$, one can observe the same caustic behaviour as on Fig. 1. Indeed, on Fig. 6(d), one can clearly observe two curves: the first one with a shape of a standard ellipse and a second one with a much more complex behaviour composed of four cusps tips located along specific orientation of the first ellipse.

By implementing this method, we have demonstrated that if the paraxial and aberration parameters of the system are first calculated, it is then possible to determine the caustic shape. Unfortunately, the estimation of optical properties takes a lot longer than the actual caustic computation. Indeed, the catastrophe theory formalism makes caustic extraction quite easy. Therefore, remembering that we began with very simple analytical forms for the axial potentials, the approach remains nevertheless limited by the estimation of the optical properties. In reality, starting with real lenses parameters (e.g. shapes, magnetization state of the pole pieces, coils currents) we will have to use finite element methods to numerically compute these potentials which will drastically increase the overall computation time. The major benefit of catastrophe theory - which lies in the simplicity of its physical approach to the understand of caustic formation - is compromised by this complex numerical process, which begins with the computation of the potentials and their derivatives and concludes with the estimation of the function L . Therefore, we do not find the method particularly

interesting in its current state, even compared to the raw solution that would require calculating each trajectory separately to extract the geometric location of the caustic.

Nevertheless, one can implement an approach based only on the properties of the generating function, without any *a priori* knowledge of the optical system parameters. Catastrophe theory actually allows us to treat any optical problem mathematically as an exercise of topology defined by state and control variables, regardless of the details of their reality. Of course, if one wish to perform a link with an experiment through a measurement - for example the size of a caustic - one has to estimate the dimensions of the control variables, and as a consequence, to compute all the optical properties (paraxial and aberrations). We thus fall back into the previous pitfall. On the other hand, one can connect our calculation to observables by comparing dimensionless data extracted from the mathematical treatment with the experiment, for example ratios between the control variables. This method constitutes, in fact, a very effective strategy that we will develop in the next section. In particular, we will see that catastrophe theory offers the possibility of an analytical treatment of optical problems that are far too complex to be analytically tackled with standard CPO formalism.

D. Application: analytical derivation of caustic geometry using catastrophe theory with no *a priori* knowledge

1. System with rotationally symmetry

Our starting point will be the rotationally symmetric system that restricts the optical path expansion to the two coefficients C_s and C_{df} . Considering first $C_s = 0$ the generating function can be written in its most simplest form as follow :

$$\Phi(x_a, y_a, C_1, C_2, C_3) = C_1 x_a + C_2 y_a + C_3 (x_a^2 + y_a^2) \quad (117)$$

with:

$$C_1 = -\frac{x}{z} \quad (118)$$

$$C_2 = -\frac{y}{z} \quad (119)$$

$$C_3 = \frac{C_{df}}{2u_{aa}^2} + \frac{1}{2z} \quad (120)$$

All control variables have been previously described in equations (105) to (113). The equilibrium surface is therefore given by:

$$\begin{cases} \frac{\partial \Phi}{\partial x_a} = C_1 + 2C_3 x_a = 0 \\ \frac{\partial \Phi}{\partial y_a} = C_2 + 2C_3 y_a = 0 \end{cases} \quad (121)$$

$$\begin{cases} \frac{\partial \Phi}{\partial x_a} = C_1 + 2C_3 x_a = 0 \\ \frac{\partial \Phi}{\partial y_a} = C_2 + 2C_3 y_a = 0 \end{cases} \quad (122)$$

In that situation, $C_3 = 0$ provides the only root of the Hessian, which - when plugged into (121) and (122) - yields $(C_1, C_2) = (0, 0)$ which correspond to $x = y = 0$ in real space. Hence, all rays defined by any set of pupil coordinates (x_a, y_a) will cross at this point. This is the well known definition of paraxial image plane located at $z_g = -u_{\alpha a}^2/C_{df}$. This simple example has the benefit of showing how analytical manipulation of the generating function can yield significant optical knowledge.

Adding the spherical aberration, the generating function becomes:

$$\Phi(x_a, y_a, C_1, C_2, C_3) = C_1 x_a + C_2 y_a + C_3(x_a^2 + y_a^2) + x_a^4 + 2x_a^2 y_a^2 + y_a^4 \quad (123)$$

As done previously, one can calculate the equilibrium surface by differentiating Φ :

$$\begin{cases} \frac{\partial \Phi}{\partial x_a} = C_1 + 2C_3 x_a + 4x_a^3 + 4x_a y_a^2 = 0 \\ \frac{\partial \Phi}{\partial y_a} = C_2 + 2C_3 y_a + 4x_a^2 y_a + 4y_a^3 = 0 \end{cases} \quad (124)$$

$$\begin{cases} \frac{\partial \Phi}{\partial x_a} = C_1 + 2C_3 x_a + 4x_a^3 + 4x_a y_a^2 = 0 \\ \frac{\partial \Phi}{\partial y_a} = C_2 + 2C_3 y_a + 4x_a^2 y_a + 4y_a^3 = 0 \end{cases} \quad (125)$$

which leads to the degenerate set:

$$\det(H[\Phi]) = 48x_a^4 + 96x_a^2 y_a^2 + 48y_a^4 + 32C_3(x_a^2 + y_a^2) + 4C_3^2 = 0 \quad (126)$$

Carrying out a change of variable $X = x_a^2 + y_a^2$, equation (126) can be re-written as:

$$48X^2 + 32C_3 X + 4C_3^2 = 0 \quad (127)$$

which admits two solutions:

$$\begin{cases} X_1 = \frac{-C_3}{2} \\ X_2 = \frac{-C_3}{6} \end{cases} \quad (128)$$

$$\begin{cases} X_1 = \frac{-C_3}{2} \\ X_2 = \frac{-C_3}{6} \end{cases} \quad (129)$$

By definition, X has to be positive, thus equation (126) does not have any solution if $C_3 > 0$. Therefore, a caustic can be observed if and only if $C_3 \leq 0$, for instance before the Gaussian plane $z < z_g$ when $C_s > 0$. We then retrieve a well known result but expressed within a more general condition.

One can also identify the location of the two roots mapped into the pupil plane using the equation of a circle $x_a^2 + y_a^2 = X_i$ ($i = (1, 2)$). We have thus demonstrated analytically the origin of the two red circles first encountered on Fig. 7(a). The small one is associated to the X_2 solution corresponding to a radius $\sqrt{-C_3/6}$, while the larger one corresponds to the X_1 solution defined by a radius of $\sqrt{-C_3/2}$. Going back to the equilibrium surface (124) and (125), we may determine the caustics generated by these X_1 and X_2 solutions by projecting their locations in the equilibrium surface onto the control

space. To this aim, let's define (C_{1i}, C_{2i}) the set of control variables which define the caustic function extracted from the solution X_i . Knowing that $x_a^3 = x_a X_i - y_a^2 x_a$ and $y_a^3 = y_a X_i - x_a^2 y_a$, we can write the equilibrium surface as:

$$\begin{cases} \frac{\partial \Phi}{\partial x_a} = 4x_a X_i + 2C_3 x_a + C_{1i} \\ \frac{\partial \Phi}{\partial y_a} = 4y_a X_i + 2C_3 y_a + C_{2i} \end{cases} \quad (130)$$

$$\begin{cases} \frac{\partial \Phi}{\partial x_a} = 4x_a X_i + 2C_3 x_a + C_{1i} \\ \frac{\partial \Phi}{\partial y_a} = 4y_a X_i + 2C_3 y_a + C_{2i} \end{cases} \quad (131)$$

Hence the caustic generated by the X_1 solution corresponds to a point located at $(C_1, C_2) = (0, 0)$ i.e. $x = y = 0$. In order to extract the caustic generated by the X_2 solution, we have to solve the following system:

$$\begin{cases} \frac{\partial \Phi}{\partial x_a} = \frac{4}{3}x_a C_3 + C_{12} = 0 \\ \frac{\partial \Phi}{\partial y_a} = \frac{4}{3}y_a C_3 + C_{22} = 0 \end{cases} \quad (132)$$

$$\begin{cases} \frac{\partial \Phi}{\partial x_a} = \frac{4}{3}x_a C_3 + C_{12} = 0 \\ \frac{\partial \Phi}{\partial y_a} = \frac{4}{3}y_a C_3 + C_{22} = 0 \end{cases} \quad (133)$$

which gives:

$$\begin{cases} x_a = -\frac{3C_{12}}{4C_3} \\ y_a = -\frac{3C_{22}}{4C_3} \end{cases} \quad (134)$$

$$\begin{cases} x_a = -\frac{3C_{12}}{4C_3} \\ y_a = -\frac{3C_{22}}{4C_3} \end{cases} \quad (135)$$

and therefore:

$$C_{12}^2 + C_{22}^2 = -\frac{8}{27}C_3^3 \quad (136)$$

The caustic generated by the X_2 degenerated set will then be a circle of radius $\sqrt{-8C_3^3/27}$ in the control space. These two simple examples provided aid in understanding the method's immense potential since the analytical technique provides very quickly new informations while obtaining the same optical behaviours that were previously observed using complex numerical computations. Fig. 8 shows the evolution of the caustic observed in a rotationally symmetric optics only affected by the spherical aberration, and considering an interval of the control variable $C_3 \in [-5, 0]$. Applying J. Nye's method [21], one can demonstrate that the radius of the caustic circle in the control space (C_2, C_3) will obey the equation of a canonical cusp defined in Thom's theory (see table I). The apex of this cusp is located at position $(0, 0, 0)$ of the tridimensional control space. Therefore, following [21], we find that the position given by $C_3 = 0$ corresponds to the Gaussian image plane along the optical axis $z_g = -u_{\alpha a}^2/C_{df}$. The cusp profile projected onto the (C_2, C_3) control space is also shown on Fig. 8.

2. Introduction of tilt along the optical axis: effect on the canonical cusp in real space

J. Nye also investigated the orientation and the distortion of this cusp in the control space arising from an

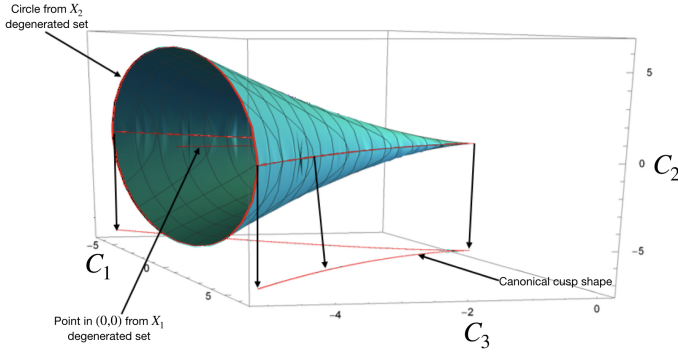


Fig. 8 Caustic of a pure rotationally symmetric optical system mapped in the control space. The two solutions X_1 and X_2 are reproduced after considering only the influence of third order spherical aberration.

optical symmetry breaking or a non-dissipative propagation within a general anisotropic and inhomogeneous medium [18]. The same procedure can be applied in CPO considering - for instance - the introduction of dipolar field Ψ_1 along the optical axis. From (82) we know that such dipolar induces an A_0 coefficient which has to be included in the control variables through the expressions (105) to (113). We notice that the generating function remains defined by only the three first control variables. Therefore, the caustic equation of the X_2 degenerated set must follow the same equation (136). In other words, nothing change within the control space due to the introduction of dipolar field.

Nevertheless, the effect of A_0 can be understood when switching from the control space to the real space. Performing this change while keeping $A_0 = 0$ first, one simply has to rewrite equation (136) by replacing C_1 and C_2 using their expressions (105) and (106):

$$x^2 + y^2 = -\frac{1}{27} \frac{(C_{df}z + u_{\alpha\alpha}^2)^3}{u_{\alpha\alpha}^2 C_s z} \quad (137)$$

The same procedure is then performed when adding A_0 in C_1 and C_2 . Equation (136) then reads:

$$\begin{cases} (x - \text{Re}(\zeta))^2 + (y - \text{Im}(\zeta))^2 \\ \quad = -\frac{1}{27} \frac{(C_{df}z + u_{\alpha\alpha}^2)^3}{u_{\alpha\alpha}^2 C_s z} \\ \quad \zeta = \frac{A_0 z}{u_{\alpha\alpha}} e^{i\chi_a} \end{cases} \quad (138)$$

$$\zeta = \frac{A_0 z}{u_{\alpha\alpha}} e^{i\chi_a} \quad (139)$$

To plot these equations and qualitatively observe the impact of A_0 on the caustic, we have arbitrarily set $-C_{df} = C_s = u_{\alpha\alpha} = 1$. The results are reported on Fig. 8(a) for $A_0 = 0$, and Fig. 8(b) for an arbitrary value $A_0 = -1$. These results are in agreement with the well-known observation that a dipole field Ψ_1 at first order simply tilts the optical axis. The overall geometry of the caustic remains unchanged, as it was already obvious from the control space perspective.

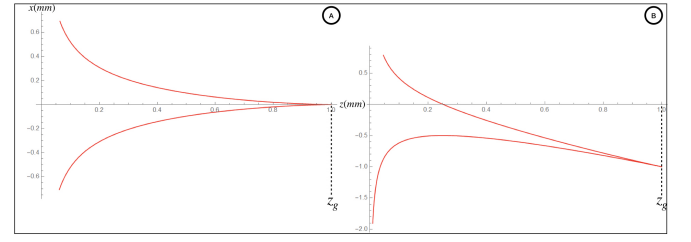


Fig. 9 Real space profile of the cusp catastrophe observed in a rotationally symmetric system with the presence of spherical aberration. A : with and B : without deflection introduced through the presence of a dipolar field component Ψ_1 .

3. System combining fields with rotational and quadrupole symmetries

As previously done, one can add a quadrupole field Ψ_2 which will induce a two-fold astigmatism term A_1 linked to Ψ_2 through (82). However, unlike the previous analysis that used optical calculations of A_1 knowing the value of Ψ_2 , we now simply use the catastrophe theory formalism to investigate the influence of this aberration, without any *a priori* knowledge of the real fields. The methodology will then be identical to that used in the previous section for the rotationally symmetric system and will consist of analysing the geometrical behaviour of the generating function within the control space.

It is crucial to note that the addition of A_1 results in an increased number of control variables (see equations (105) to (113)), making the equations denser and more challenging to interpret at a first sight. We will see for instance that the determinant of the Hessian will be written as a fourth order polynomial function. Finding the roots of this polynomial is still mathematically possible, but much more complex than in the previous quadratic situation. We have nevertheless chosen to put all the demonstrations in the main body of the paper, because here lies the beauty of this analytical approach. This makes it more difficult to read, but we shall see that - in practice - this is only due to cumbersome expressions. The essence of the reasoning remains however as simple as in the previous situation. Practically, the analytical expressions for the roots have been determined with the help of *Mathematica* software. The code is also given in the supplementary material for information.

Thus, we now examine an optical system with only C_s and A_1 aberration coefficients. The generating function can be written :

$$\begin{aligned} \Phi(x'_a, y'_a, C'_1, C'_2, C'_3, C'_4, C'_5) = & C'_1 x'_a + C'_2 y'_a \\ & + C'_3 (x'^2_a + y'^2_a) + C'_4 (x'^2_a - y'^2_a) \\ & + C'_5 x'_a y'_a + x'^4_a + 2x'^2_a y'^2_a + y'^4_a \end{aligned} \quad (140)$$

where we have noted state and control variables with a prime corresponding to an arbitrary coordinate system relative to the caustic orientation in order to simplify

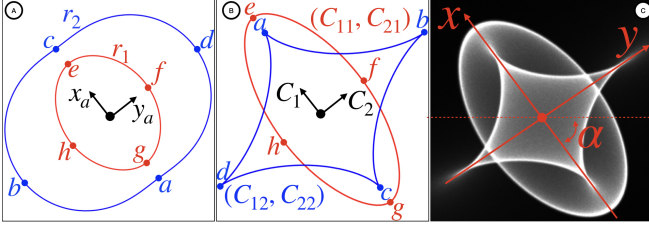


Fig. 10 A: Map of the Hessian determinant degenerated sets in the space defined by the two state variables x_a and y_a . B: Caustics obtained in the control space related to the two degenerated solutions (red and blue) depicted in A. C : Experimental caustic observed in the I2TEM microscope.

subsequent expressions. Only the C_3 coefficient remains without prime as it is not related to the caustic orientation and will then remains unchanged in the following simplifications. Using usual polar coordinates $r = \sqrt{x_a'^2 + y_a'^2}$ and θ corresponding to the argument, the generating function reads:

$$\begin{aligned} \Phi(r, \theta, C_1', C_2', C_3, C_4', C_5') &= C_1' r \cos(\theta) + C_2' r \sin(\theta) \\ &+ C_3 r^2 + C_4' (r^2 \cos^2(\theta) - r^2 \sin^2(\theta)) \\ &+ C_5' r^2 \cos(\theta) \sin(\theta) + r^4 \end{aligned} \quad (141)$$

By linking a set of new control variables to a basis defined by the caustic's symmetry, one can in practice lower the number of effective variables and simplify the problem. Indeed, Fig. 10(c) reports an example of caustic observed in the I2TEM when a quadrupole field is applied with the condensor stigmators. As shown, the two new coordinates axes (x, y) are tilted relative to the global image axis (x', y') (again the prime notations are used when orientation is unrelated to the caustic) following the natural orientation of the caustic. We have then to define the set of state and control variables attached to these main caustic axis - keeping in mind that the caustic could be rotated when A_1 changes. This is the origin of the two control variables C_4' and C_5' which physically represent this same influence emerging from the two-fold astigmatism. A_1 being a complex number, equations (108) and (109) shows that one needs two control variables to define the action of A_1 in an arbitrary reference system through its real and imaginary parts. The modulus of the complex interplay of C_4' and C_5' can then be represented by a new control variable C_4 . This new control variable is associated to the caustic coordinate system independently of the value of α - which then correspond to the argument of this complex association. Hence, from (108) and (109) one obtains:

$$C_4 = -\sqrt{C_4'^2 + \left(\frac{C_5'}{2}\right)^2} = -\frac{2|A_1|}{C_s} u_{\alpha a}^2 \quad (142)$$

$$\alpha = -\frac{\arctan\left(\frac{C_5'}{2C_4'}\right)}{2} = -\frac{\arg(A_1) + 2\chi_a}{2} \quad (143)$$

With those definitions, one can then simplify the generating function (141) after applying the following simplifica-

tion:

$$\begin{aligned} C_4' (r^2 \cos^2(\theta) - r^2 \sin^2(\theta)) \\ + C_5' r^2 \cos(\theta) \sin(\theta) = C_4 (x_a^2 - y_a^2) \end{aligned} \quad (144)$$

with:

$$\begin{cases} x_a = r \cos(\theta + \alpha) \\ y_a = r \sin(\theta + \alpha) \end{cases} \quad (145)$$

$$\quad (146)$$

Finally, we define the two new control variables (C_1, C_2) within the new coordinate system tilted by α (see Fig. 10(b)):

$$\begin{cases} C_1 = C_1' \cos(\alpha) + C_2' \sin(\alpha) \\ C_2 = C_2' \cos(\alpha) - C_1' \sin(\alpha) \end{cases} \quad (147)$$

$$\quad (148)$$

with these new coordinates, one can reconstruct the generating function in a more condensed manner using only four control variables, see Fig. 10(a) and Fig. 9(b):

$$\begin{aligned} \Phi(x_a, y_a, C_1, C_2, C_3, C_4) &= C_1 x_a + C_2 y_a + C_3 (x_a^2 + y_a^2) \\ &+ C_4 (x_a^2 - y_a^2) + x_a^4 + 2x_a^2 y_a^2 + y_a^4 \end{aligned} \quad (149)$$

Additionally, one can perform all the analysis within the restricted range $C_4 < 0$. Indeed, considering positive values of C_4 will be mathematically identical, since the generating function remains the same by simply swapping the state and control space axis i.e. $x_a \rightarrow y_a$, $y_a \rightarrow x_a$, $C_1 \rightarrow C_2$, $C_2 \rightarrow C_1$ and $C_4 \rightarrow -C_4$. The critical set can now be extracted:

$$\begin{cases} \frac{\partial \Phi}{\partial x_a} = C_1 + 2x_a(C_3 + C_4) + 4x_a^3 + 2x_a y_a^2 = 0 \\ \frac{\partial \Phi}{\partial y_a} = C_2 + 2y_a(C_3 - C_4) + 2x_a^2 y_a + 4y_a^3 = 0 \end{cases} \quad (150)$$

$$\quad (151)$$

and the degenerated set:

$$\frac{\partial f}{\partial x_a} \frac{\partial \Phi}{\partial y_a} - \left(\frac{\partial \Phi}{\partial x_a \partial y_a} \right)^2 = 0 \quad (152)$$

are found by extracting the roots of this fourth order polynomial function:

$$\begin{aligned} 48x_a^4 + 96x_a^2 y_a^2 + 48y_a^4 + 32C_3(x_a^2 + y_a^2) \\ - 16C_4(x_a^2 - y_a^2) + 4(C_3^2 - C_4^2) = 0 \end{aligned} \quad (153)$$

which is more conveniently written in polar coordinates:

$$48r^4 + (32C_3 - 16C_4 \cos(2\theta))r^2 + 4(C_3^2 - C_4^2) = 0 \quad (154)$$

Considering $X = r^2$, the determinant of the Hessian corresponds to a second order polynomial function, which roots can easily be found. Using our **Mathematica** script given in supplementary material, we obtain the two degenerated sets:

$$r_1 = \frac{\sqrt{-2C_3 + C_4\cos(2\theta) - \sqrt{C_3^2 + 3C_4^2 - 4C_3C_4\cos(2\theta) + C_4^2\cos^2(2\theta)}}}{\sqrt{6}} \quad (155)$$

$$r_2 = \frac{\sqrt{-2C_3 + C_4\cos(2\theta) + \sqrt{C_3^2 + 3C_4^2 - 4C_3C_4\cos(2\theta) + C_4^2\cos^2(2\theta)}}}{\sqrt{6}} \quad (156)$$

These solutions are shown on Fig. 10(a), where the red (respectively blue) curve corresponds to r_1 (r_2). From these solutions one can extract the caustic shape within

the control space by solving the Fermat's principle. As done previously, we define a parametric equation for each solutions expressed in (C_{1i}, C_{2i}) for the set r_i :

$$C_{11} = \frac{\sqrt{-4C_3 + 2C_4\cos(2\theta) - \sqrt{2}\sqrt{2C_3^2 + 7C_4^2 - 8C_3C_4\cos(2\theta) + C_4^2\cos(4\theta)}}}{6\sqrt{3}} \times \left(-2C_3 - 6C_4 - 2C_4\cos(2\theta) + \sqrt{2}\sqrt{2C_3^2 + 7C_4^2 - 8C_3C_4\cos(2\theta) + C_4^2\cos(4\theta)} \right) \cos(\theta) \quad (157)$$

$$C_{21} = \frac{\sqrt{-4C_3 + 2C_4\cos(2\theta) - \sqrt{2}\sqrt{2C_3^2 + 7C_4^2 - 8C_3C_4\cos(2\theta) + C_4^2\cos(4\theta)}}}{6\sqrt{3}} \times \left(-2C_3 + 6C_4 - 2C_4\cos(2\theta) + \sqrt{2}\sqrt{2C_3^2 + 7C_4^2 - 8C_3C_4\cos(2\theta) + C_4^2\cos(4\theta)} \right) \sin(\theta) \quad (158)$$

$$C_{12} = -\frac{\sqrt{-4C_3 + 2C_4\cos(2\theta) + \sqrt{2}\sqrt{2C_3^2 + 7C_4^2 - 8C_3C_4\cos(2\theta) + C_4^2\cos(4\theta)}}}{6\sqrt{3}} \times \left(2C_3 + 6C_4 + 2C_4\cos(2\theta) + \sqrt{2}\sqrt{2C_3^2 + 7C_4^2 - 8C_3C_4\cos(2\theta) + C_4^2\cos(4\theta)} \right) \cos(\theta) \quad (159)$$

$$C_{22} = -\frac{\sqrt{-4C_3 + 2C_4\cos(2\theta) + \sqrt{2}\sqrt{2C_3^2 + 7C_4^2 - 8C_3C_4\cos(2\theta) + C_4^2\cos(4\theta)}}}{6\sqrt{3}} \times \left(2C_3 - 6C_4 + 2C_4\cos(2\theta) + \sqrt{2}\sqrt{2C_3^2 + 7C_4^2 - 8C_3C_4\cos(2\theta) + C_4^2\cos(4\theta)} \right) \sin(\theta) \quad (160)$$

Two pairs of parametric equations are then provided by the catastrophe theory, enabling us to examine an optical system containing quadrupolar and rotationally symmetric fields without ever requiring a quantitative estimate of their values. Yet, we are aware that this is still feasible in the present case only because the polynomial is below order five - which enables analytical solutions for the roots. Nevertheless, the situation studied here is, in practice, what is mostly observed in a electron and ion microscopy experiments. The main exceptions being the cases where an aberration corrector drastically reduces the contribution of C_s so that the introduction of aberrations B_2 , A_2 , and higher becomes necessary.

We will now look at the information that can be extracted from this pair of solutions. We will see that some interesting details that would have been difficult, if not

impossible, to find using the numerical method, can be extracted from these solutions. The caustic generated using r_1 falls within the classic definition of a *fold* while the one generated using r_2 set creates four *cusps* in the control space (see Fig. 10) [11]. To facilitate the discussion, in the following we will refer to them as *fold-caustic* and *cusp-caustic* respectively.

The correspondence between the rays positions within the two caustics and their locations in the pupil plane can now be established. To do so, let's define ϕ , the angle associated to a random point (C_{1i}, C_{2i}) located on one of the two caustics solutions $i = (1, 2)$ and relatively to the control space main axis (C_1, C_2) . Equations (157), (158), (159) and (160) can then be simply written as $C_{1i} = g_{(1i)}\cos(\theta)$, $C_{2i} = g_{(2i)}\sin(\theta)$, where $g_{(ni)}$ denote monotonic functions. We then obtain the following relations between some specific orientations of the degenerated set in the pupil plane and the two caustics

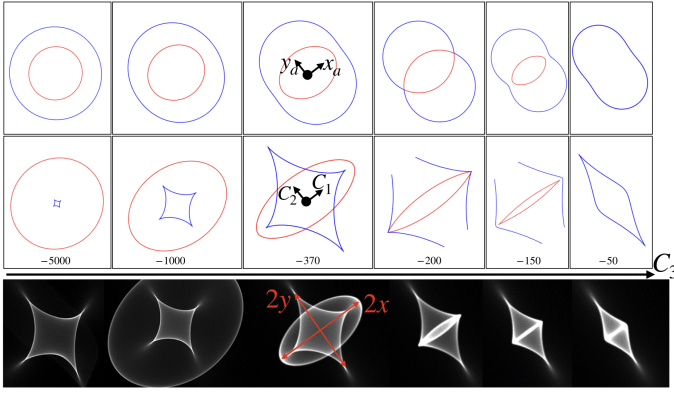


Fig. 11 A: Evolution of the Hessian determinant degenerated sets with C_3 control variable. B: Evolution of the associated caustics in the control space. C: Evolution of the experimental caustic observed in the I2TEM microscope by changing the defocus parameter C_{df} , linked to the C_3 control variable through (120).

in the control space:

$$\begin{aligned} \theta \in \left\{-\frac{\pi}{2}, \frac{\pi}{2}\right\} &\implies C_{1i} = 0 \implies \psi \in \left\{-\frac{\pi}{2}, \frac{\pi}{2}\right\} \\ \theta \in \{0, \pi\} &\implies C_{2i} = 0 \implies \psi \in \{0, \pi\} \end{aligned} \quad (161)$$

The exact locations of the cardinal points - which corresponds to the points along the two axis of symmetry - depend on the sign of the control variables $C_{ji}(\theta)$. We can show that in most cases we have $\theta = \psi$. These cardinal points are highlighted on Fig. 9(a) and Fig. 9(b) by letters ranging from b, d, e, f, g . An inversion is observed for the cusp-caustic when $\theta = \pm\pi/2$ leading to $\psi = \mp\pi/2$. These two specific locations are noted a, c on Fig. 9(a) and Fig. 9(b). Additionally, one can show that these cardinal points can be specified only for a certain range of C_3 . In particular, these cardinal points can be defined for the fold-caustic only if $C_3 < C_4$ but only when $C_3 < -C_4$ for the cusp-caustic. Going back to the real space, these two limits simply represent the sagittal and the tangential focal points defined $z_{s/t} = -\frac{u_{\alpha\alpha}^2}{\pm|A_1| + C_{df}}$.

The general behaviour of these caustics as a function of C_3 can be intuitively understood by plotting them - which constitutes a quick and easy task from the previously-derived analytical solutions. For example, Fig. 10 displays the evolution of a caustic within the (C_1, C_2) control space calculated for an arbitrary two-fold astigmatism represented by the control variable $C_4 = -100$. The caustic is observed for different values of C_3 , which physically corresponds to a translation along the optical axis, i.e. a defocus. Experimental data are also shown for a qualitative comparison. We have chosen not to include any scales, as these would be of no real physical interest. Indeed, as it was discussed earlier, in this catastrophe theory method, we are only concerned with the evolution of the relative dimensions and symmetries between the morphologies of the two solutions within the control space. Keeping this in mind,

we can assess the agreement between the plots of these solutions in (C_1, C_2) space as a function of C_3 and the experimental data acquired with the I2TEM microscope - for a non-zero astigmatism A_1 . The caustics evolution has been acquired by slightly changing the focal strength of the condenser system (in the present example, the first condenser lens).

By developing the two solutions using the (C_{1i}, C_{2i}) parametric equations (157) to (160), one can obtain exact relationships linking measurable geometrical parameters of the caustic - extracted for specific C_3 parameters. Such relationships, which depend on the aberration coefficients, can be fairly simple. The scenario defined by $C_3 = 2C_4$, for example, is relevant to some practical considerations. Indeed, along the C_1 axis, the fold-caustic and the cusp-caustic eventually share two cardinal points at this specific $C_3 = 2C_4$ location. The scenario is clearly observed on Fig. 10 for $C_3 = -200$. At this specific point we can extract the relationship $C_{11}(\theta = 0) = C_{12}(\theta = 0) = -2C_4\sqrt{-2C_4}$, which can be written in real space as:

$$\frac{x}{z} = \frac{4|A_1|^{\frac{3}{2}}}{|u_{\alpha\alpha}|\sqrt{C_s}} \quad (162)$$

Besides, the condition $C_3 = 2C_4$ between the control parameters implies that $-2z(C_{df} + 2|A_1|) = 1$. Thus, we could for instance design an experiment where a two-fold astigmatism A_1 and a defocus C_{df} are manually introduced to match this condition $C_3 = 2C_4$ - the proper value for the defocus corresponding to a contact between the "cusp-caustic" and the "fold-caustic". Then, one can easily find the value of this defocus, which gives access to the value of A_1 . Knowing this value, and using the relationship (162), one can precisely extract the spherical aberration parameter C_s . To do so however, one needs to eliminate the term $u_{\alpha\alpha}$ - corresponding to the position of the marginal ray in the pupil plane - through e.g. two subsequent measurements using two different condenser apertures.

We have thus demonstrated that a simple relation between the coefficients could be derived using catastrophe theory, which would have been challenging to extract using a brute force numerical approach. The condition $C_3 = 2C_4$ is however quite specific. We will now work out another simple relation in a more general situation. Let's examine the set of positions in the control space - along the optical axis - defined by $C_3 < 2C_4$, as shown on Fig. 10. The relations (157) to (160) enable us to establish a relationship between the two perpendicular directions x, y given by the larger dimensions of the fold and cusp caustics, respectively:

$$\frac{C_{11}(\theta = 0)}{C_{22}(\theta = -\pi/2)} = \frac{C_3 + C_4}{2\sqrt{3}C_4} \quad (163)$$

Therefore, a simple measurement of these distances leads to the following relation between the defocus and two-fold

astigmatism:

$$\frac{x}{y} = \frac{2z(C_{df} - |A_1|) + 2u_{\alpha\alpha}}{-6\sqrt{2}|A_1|} \quad (164)$$

In summary, we have chosen to highlight two specific situations - encapsulated in equations (162) and (164) - to illustrate the strength of CCPO. Although we haven't used these relationships experimentally yet, we intend to conduct specific TEM experiments to test our approach before implementing it on a FIB instrument - where measuring aberrations is a significant technological difficulty.

The aim of this work was to show the great potential offered by the mathematical framework of catastrophe theory. First of all, and this is far more important to us than any applications, the approach developed by R. Thom opens up a completely new window of opportunity for understanding these complex figures that we all observe in our every day. Furthermore, the universal character of this theory enable us to make very meaningful analogies between the field of optics and other fields of physical science where bifurcations can also be observed.

Indeed, the relations obtain in the latter part of this article - namely (162) and (164) - convey a very universal character as they must also be valid in any system characterized by the same generating function. In the context of CPO, they offer a fresh and new insight into the detection of aberrations, for instance in focused ion beam systems.

It must be stressed that such a purely analytical approach is however limited to a small number of aberration coefficients - since from order five onwards it would no longer be possible to define the roots of the determinant of the Hessian univocally. Nevertheless, we believe that by playing with experimentally free parameters - such as defocus C_{df} , two-fold A_1 and three-fold A_2 astigmatisms - it should be always possible to define a situation where the dimensionality of the control space remains restricted below five.

V. Conclusion

We applied the formalism of catastrophe theory to a charged particle optics problem by adapting the classical eikonal theory into the geometrical language originally developed by R. Thom. This formalism allowed us to reproduce the behaviour of optical caustics analytically without any *a priori* knowledge of our optics. We were able to gauge the efficiency of this innovative method by comparing these results with those obtained directly from the eikonal formalism. We were thus able to reproduce the caustics observed in a TEM containing spherical aberration and axial astigmatism without having to calculate the distribution of electromagnetic potentials inside each optical element. It is in this highly computational phase that traditional methods require strong resources. Indeed, estimating these potentials remains unfortunately

necessary if caustics have to be evaluated by the eikonal method and a fortiori using conventional ray tracing. For example, these calculations are too time-consuming to be used for actual measurements during investigations if one wishes to rapidly extract the aberrations from caustics in order to optimize the alignment of an instrument. The new mathematical expressions established during this work offer a whole new paradigm because their estimations are almost instantaneous. The geometric approach of catastrophe theory should then enable us in the future to perform quick measurements of the optical properties of various systems using charged particles. We are now mainly considering applications to electrostatic optics which are the heart of ion microscopes like FIB or SIMS. The nature of ions makes the application of usual optical characterization methods, widely used in electron optics, very complex, if not impossible. Caustics observed by etching and then analysed by catastrophe theory take a few milliseconds, paving the way for live measurement of the optical properties in future ions-based instruments, which is a first step towards optimizing their optics.

Acknowledgments

This study has been supported through the grant NanoX n° ANR-17-EURE-0009 in the framework of the "Programme des Investissements d'Avenir". We also acknowledge financial support by the European Union's Horizon Europe framework program for research and innovation under grant agreement n° 101094299 (IMPRESS project).

References

- [1] Thomas Kiser, Michael Eigensatz, Minh Man Nguyen, Philippe Bompas, and Mark Pauly. Architectural Caustics — Controlling Light with Geometry. In Lars Hesselgren, Shrikant Sharma, Johannes Wallner, Niccolo Baldassini, Philippe Bompas, and Jacques Raynaud, editors, *Advances in Architectural Geometry 2012*, pages 91–106. Springer Vienna, Vienna, 2013.
- [2] William Rowan Hamilton. On a General Method of expressing the Paths of Light and of the Planets by the Coefficients of a Characteristic Function. *Dublin University Review and Quarterly Magazine*, (1):795, 1833.
- [3] Florence Martin-Robine. *Histoire du principe de moindre action: trois siècles de principes variationnels de Fermat à Feynman*. Vuibert, Paris, 2006.
- [4] J.L. Synge. *Geometrical Optics: An Introduction to Hamilton's Method*. Cambridge university press edition, 1937.
- [5] H. A. Buchdahl. *An introduction to Hamiltonian optics*. Cambridge monographs on physics. Cambridge University Press, Cambridge, 1970.
- [6] R. K. Luneburg. *Mathematical theory of optics*. Univ of california press, S.l., 2021. OCLC: 1155214091.

- [7] J. F. Nye. *Natural focusing and fine structure of light: caustics and wave dislocations*. Institute of Physics Pub, Bristol ; Philadelphia, 1999.
- [8] Douglas Cline. *Variational principles in classical mechanics*. University of Rochester River Campus Libraries, Rochester, NY, revised second edition edition, 2019. OCLC: 1114330490.
- [9] René Thom. Stabilité structurelle et morphogénèse. *Poetics*, 3(2):7–19, January 1974.
- [10] Vladimir I. Arnold. *Catastrophe Theory*. Springer Berlin Heidelberg, Berlin, Heidelberg, 1992.
- [11] Eric C. Zeeman. *Catastrophe theory: selected papers, 1972 - 1977*. Addison-Wesley, Reading, Mass, 3. print edition, 1977.
- [12] Tim Poston and Ian Stewart. *Catastrophe Theory and Its Applications*. Courier Corporation, January 1996. Google-Books-ID: 7Zm5zTh8rLAC.
- [13] M. V. Berry and C. Upstill. IV Catastrophe Optics: Morphologies of Caustics and Their Diffraction Patterns. In E. Wolf, editor, *Progress in Optics*, volume 18, pages 257–346. Elsevier, January 1980.
- [14] Markus Selmke. Bubble optics. *Applied Optics*, 59(1):45, January 2020.
- [15] Harald H. Rose. *Geometrical charged-particle optics*. Number v. 142 in Springer series in optical sciences. Springer, Berlin, 2009. OCLC: ocn268931877.
- [16] A. Torre. *Linear ray and wave optics in phase space: bridging ray and wave optics via the Wigner phase-space picture*. Elsevier, Amsterdam ; Boston, 1st ed edition, 2005. OCLC: ocm60835684.
- [17] Sergio Barbero, Arthur Bradley, Norberto López-Gil, Jacob Rubinstein, and Larry Thibos. Catastrophe optics theory unveils the localised wave aberration features that generate ghost images. *Ophthalmic and Physiological Optics*, 42(5):1074–1091, September 2022.
- [18] J.F. Nye and J.H. Hannay. The Orientations and Distortions of Caustics in Geometrical Optics. *Optica Acta: International Journal of Optics*, 31(1):115–130, January 1984.
- [19] J F Nye. The catastrophe optics of liquid drop lenses. *Proceedings of the Royal Society of London. A. Mathematical and Physical Sciences*, 403(1824):1–26, January 1986.
- [20] M.V. Berry. Waves and Thom’s theorem. *Advances in Physics*, 25(1):1–26, January 1976.
- [21] J F Nye. The relation between the spherical aberration of a lens and the spun cusp diffraction catastrophe. *Journal of Optics A: Pure and Applied Optics*, 7(3):95–102, January 2005.
- [22] Walter Appel, Emmanuel Kowalski, and Walter Appel. *Mathematics for physics and physicists*. Princeton Univ. Press, Princeton, NJ, 2007.
- [23] Martin Golubitsky. An Introduction to Catastrophe Theory and Its Applications. *SIAM Review*, 20(2):352–387, April 1978.
- [24] Theodor Bröcker. *Differentiable Germs and Catastrophes*. Cambridge University Press, 1 edition, July 1975.
- [25] M Deakin. An elementary approach to catastrophe theory. *Bulletin of Mathematical Biology*, 40(4):429–450, 1978.
- [26] E. C. Zeeman. Euler buckling. In Peter Hilton, editor, *Structural Stability, the Theory of Catastrophes, and Applications in the Sciences*, volume 525, pages 373–395. Springer Berlin Heidelberg, Berlin, Heidelberg, 1976. Series Title: Lecture Notes in Mathematics.
- [27] C. H. Waddington. *Biological Process in Living Systems: Toward a Theoretical Biology*. Routledge, 1 edition, September 2017.
- [28] Alessandro Cazzolli, Diego Misseroni, and Francesco Dal Corso. Elastica catastrophe machine: theory, design and experiments. *Journal of the Mechanics and Physics of Solids*, 136:103735, March 2020.
- [29] E. C. Zeeman. Catastrophe Theory. *Scientific American*, 234(4):65–83, April 1976.
- [30] J F Nye. Symmetrical optical caustics. *Journal of Optics*, 20(7):075612, July 2018.
- [31] V. I. Arnold, editor. *Theory of singularities and its applications*. Number 1 in Advances in Soviet mathematics. American Mathematical Society, Providence, R.I, 1990.
- [32] Heinrich Bruns. Das Eikonal. *S. Hirzel*, 21(5):323, 1895.
- [33] Peter W. Hawkes and Erwin Kasper. *Principles of electron optics. Volume 1: Basic geometrical optics*. Elsevier, London, second edition edition, 2018.
- [34] P.A. Sturrock. Perturbation characteristic functions and their application to electron optics. *Proceedings of the Royal Society of London. Series A. Mathematical and Physical Sciences*, 210(1101):269–289, December 1951.
- [35] Walter Glaser. Zur Bildfehlertheorie des Elektronenmikroskops. *Zeitschrift für Physik*, 97(3):177–201, March 1935.
- [36] Miklos Szilagyi. *Electron and Ion Optics*. Springer US, Boston, MA, 1988.
- [37] Cornelius Lanczos. *The Variational principles of mechanics*. Dover Publ, New York, 4. ed., [unabridged and unaltered republ. dover ed.] edition, 1986.
- [38] m is the relativistic mass $m = \gamma m_e$, γ being the Lorentz factor, m_e the mass of the electron at rest.
- [39] H. Rose. Hamiltonian magnetic optics. *Nuclear Instruments and Methods in Physics Research Section A: Accelerators, Spectrometers, Detectors and Associated Equipment*, 258(3):374–401, August 1987.
- [40] H. A. Buchdahl. *An introduction to Hamiltonian optics*. Dover classics of science and mathematics. Dover Publications, New York, 1993.
- [41] Mikhail Yavor. *Optics of charged particle analyzers*. Number v.157 in Advances in imaging and electron physics. Academic Press, Amsterdam London, 2009.
- [42] P. Grivet. *Electron optics. Part 1, Optics*. Pergamon Press Ltd., Oxford [England], second (revised) english edition edition, 1972. OCLC: 899003663.
- [43] Walter T. Welford. *Aberrations of the symmetrical optical system*. Acad. Press, London, 1974.
- [44] Shinobu Uno, Kazuhiro Honda, Natsuko Nakamura, Miyuki Matsuya, and Joachim Zach. Aberration correction and its automatic control in scanning electron microscopes. *Optik*, 116(9):438–448, September 2005.
- [45] P. W. Hawkes. *Springer Tracts in Modern Physics, Volume 42*, volume 42 of *Springer Tracts in Modern Physics*. Springer Berlin Heidelberg, Berlin, Heidelberg, 1966.
- [46] P. W. Hawkes. *Magnetic electron lenses*. Springer-Verlag, Berlin, 1982. OCLC: 680001010.
- [47] Florent Houdellier. *Coherent electron microscopy: designing faster and brighter electron sources*. Number volume 227 in Advances in imaging and electron physics. Academic Press, London San Diego, CA Cambridge, MA Kidlington, Oxford, 2023.
- [48] Heiko Müller, Ingo Maßmann, Stephan Uhlemann, Peter Hartel, Joachim Zach, and Maximilian Haider. Aplanatic imaging systems for the transmission electron microscope.

Nuclear Instruments and Methods in Physics Research Section A: Accelerators, Spectrometers, Detectors and Associated Equipment, 645(1):20–27, July 2011.

- [49] J. Callahan. Special Bifurcations of the Double Cusp. *Proceedings of the London Mathematical Society*, s3-45(2):227–257, September 1982.
- [50] Vladimir I Arnol'd. Critical points of smooth functions and their normal forms. *Russian Mathematical Surveys*, 30(5):1–75, October 1975.
- [51] Hermann Wollnik. *Optics of Charged Particles*. Elsevier Science, Saint Louis, 2014. OCLC: 1044728471.